NETWORKS AND HETEROGENEOUS MEDIA
©American Institute of Mathematical Sciences
Volume **5**, Number **2**, June **2010**

doi:10.3934/nhm.2010.5.217

pp. **217–256**

A MATHEMATICAL MODEL FOR DYNAMIC WETTABILITY ALTERATION CONTROLLED BY WATER-ROCK CHEMISTRY

Steinar Evje*

University of Stavanger (UiS), 4036 Stavanger, Norway

Aksel Hiorth

International Research Institute of Stavanger (IRIS)
Prof. Olav Hanssensvei 15, NO-4068 Stavanger, Norway

(Communicated by Kenneth Karlsen)

Abstract. Previous experimental studies of spontaneous imbibition on chalk core plugs have shown that seawater may change the wettability in the direction of more water-wet conditions in chalk reservoirs. One possible explanation for this wettability alteration is that various ions in the water phase (sulphate, calcium, magnesium, etc.) enter the formation water due to molecular diffusion. This creates a non-equilibrium state in the pore space that results in chemical reactions in the aqueous phase as well as possible water-rock interaction in terms of dissolution/precipitation of minerals and/or changes in surface charge. In turn, this paves the way for changes in the wetting state of the porous media in question. The purpose of this paper is to put together a novel mathematical model that allows for systematic investigations, relevant for laboratory experiments, of the interplay between (i) two-phase water-oil flow (pressure driven and/or capillary driven); (ii) aqueous chemistry and water-rock interaction; (iii) dynamic wettability alteration due to water-rock interaction.

In particular, we explore in detail a 1D version of the model relevant for spontaneous imbibition experiments where wettability alteration has been linked to dissolution of calcite. Dynamic wettability alteration is built into the model by defining relative permeability and capillary pressure curves as an interpolation of two sets of end point curves corresponding to mixed-wet and water-wet conditions. This interpolation depends on the dissolution of calcite in such a way that when no dissolution has taken place, mixed-wet conditions prevail. However, gradually there is a shift towards more water-wet conditions at the places in the core where dissolution of calcite takes place. A striking feature reflected by the experimental data found in the literature is that the steady state level of oil recovery, for a fixed temperature, depends directly on the brine composition. We demonstrate that the proposed model naturally can explain this behavior by relating the wettability change to changes in the mineral composition due to dissolution/precipitation. Special attention is paid to the effect of varying, respectively, the concentration of SO_4^{2-} ions and Mg^{2+} ions in seawater like brines. The effect of changing the temperature is also demonstrated and evaluated in view of observed experimental behavior.

2000 *Mathematics Subject Classification.* Primary: 76T10, 76N10, 65M12, 35L65.

Key words and phrases. water-rock interaction, aqueous chemistry, precipitation, dissolution, spontaneous imbibition, countercurrent flow, wettability alteration .

The authors acknowledge BP, ConocoPhillips, and the Ekofisk Coventurers, including TOTAL, ENI, Hydro, Statoil and Petoro, for supporting the work through the research center COREC. Support for Steinar Evje was provided by AS Norske Shell through a sponsored professorship.

*Corresponding author.

1. Introduction.

Background information. Seawater has been injected into the naturally fractured Ekofisk chalk reservoir in the North Sea for nearly 20 years with great success. Many laboratory studies of spontaneous imbibition tests with chalk cores indicate that seawater has the potential to improve oil recovery. This has motivated for a number of experimental studies where the oil recovery for different core plugs is studied as a function of brine composition and temperature [37, 39, 38, 4, 5, 46, 40, 47]. In particular, it has been observed that the ions Mg^{2+}, SO_4^{2-}, and Ca^{2+} seem to play an important role. By varying the concentration of these ions (one at a time) in seawater like brines, different oil recovery curves are produced. In order to illustrate this, we briefly review some highly interesting experimental spontaneous imbibition results reported in [46, 47]. In Fig. 1 oil recovery curves for some imbibition experiments with chalk core plugs are shown. In the left figure results for brines with varying concentrations of SO_4^{2-} are shown. In particular, for a fixed temperature of $T = 130°C$ it is observed that increasing the amount of SO_4^{2-} ions gives a higher oil recovery level. Similar observations can be made from the right figure. One observation is that increasing the temperature for a given brine tends to increase the oil recovery. Another is that for a temperature at $T = 100°C$, adding Mg^{2+} ions to the imbibing brine leads to a strong increase in the oil recovery. When temperature is $T = 130°C$, this increase in oil recovery is amplified. This characteristic behavior also seems to depend on the amount of SO_4^{2-} ions that are present. In view of these experimental observations the purpose of this paper is to deal with the following questions:

- Firstly, how to explain that different (steady state) oil recovery levels are reached depending on the chosen brine composition? What is the fundamental mechanism behind this behavior?
- Secondly, how to explain that increase of respectively, SO_4^{2-} ions and Mg^{2+} ions in the imbibing brine, give higher oil recovery levels?

Main idea. More precisely, the objective of this work is to bring forth a mathematical model that can allow for systematic and quantitative studies of the relation between brine composition and produced oil as observed in a lab scale setting. This will be achieved by combining two different modeling components:

(i) Modeling of water-rock interaction in the context of geo-chemistry.
(ii) Modeling of two-phase water-oil transport effects by means of relative permeability and capillary pressure curves.

Highly sophisticated models have been developed for description of water-rock interaction governed by various transport effects (convective transport, molecular diffusion, mechanical dispersion, etc), see for example [25, 36, 29, 31] and references therein for a nice overview of this very active research field. However, this research is typically in the context of water-ion-mineral systems (single-phase systems).

On the other hand, petroleum research has been a driving force behind development of modeling of two-phase water-oil transport (more generally, multiphase flow in porous media) [15]. Modeling and experimental activity have walked hand in hand for decades. See for instance [35, 18, 34] for some interesting and recent examples where modeling and experimental activity are both included in the study of spontaneous imbibition processes on lab scale. However, the coupling between (i) and (ii) seems to be more rare. It is our belief that we have to carefully design

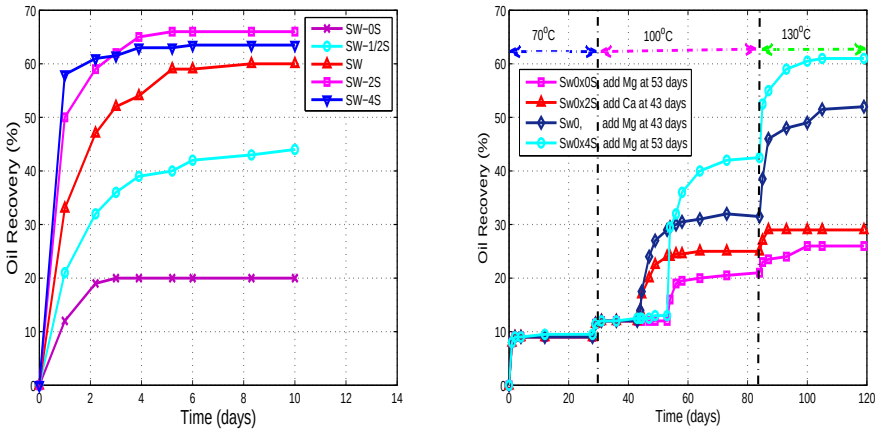

FIGURE 1. **Left**: Oil recovery curves for imbibition tests on chalk cores performed at 130°C at various SO_4^{2-} concentrations in the imbibing fluids. SW represents seawater whereas SW-0S represents seawater without SO_4^{2-}, SW-2S represents seawater with 2 times seawater concentration of SO_4^{2-}, and so on. **Right**: Oil recovery curves for imbibition tests on chalk cores where Mg^{2+} or Ca^{2+} are added to the imbibing brine. Sw0 represents seawater without Mg^{2+} and Ca^{2+} whereas Sw0x0S is the same seawater but without SO_4^{2-}, Sw0x2S contains 2 times seawater concentration of SO_4^{2-}, and so on. Change of temperature is also involved. Figures have been reproduced, respectively, from the work [46] (left figure) and [47] (right figure) by the accuracy of an eye and must be considered as approximate.

models that combine (i) and (ii) in an appropriate manner in order to obtain models that can explain the relation between oil recovery curves and brine composition, as reflected by Fig. 1.

At this stage, as far as the core scale model is concerned, various simplifications will be done in order to not arrive at an overly complicated model with many different parameters that can be tuned. However, the hope is that yet the model will be sophisticated enough to suggest nontrivial mechanisms that possibly play a role in the relatively complicated physico-chemical system we are dealing with. In particular, a mathematical model that integrates (i) and (ii) can represent a helpful tool for improved understanding of the experimental results. The main idea we have implemented is formulation of a mathematical model that includes:

- two phase water-oil displacement (pressure driven and/or capillary driven);
- aqueous chemistry and water-rock interaction;
- dynamic wettability alteration, in terms of changes in relative permeability and capillary pressure curves, that is linked to the water-rock interaction.

In view of calculations based on thermodynamic equilibrium chemistry [21, 22] where a linear correlation between oil recovery and dissolution of calcite is obtained, a natural choice is to link wettability alteration to dissolution of calcite. This line will be pursued in this work. However, it should be noted that the framework we

work within is general enough to explore different possible relations between water-rock interaction (dissolution/precipitation and/or surface chemistry) and changes in the flow functions (relative permeability and capillary pressure).

A key point in the present work is to link the water-rock chemistry to changes in the wetting state. In particular, we do no attempt to include details of the oil chemistry. Oil chemistry is implicitly taken care of in a more rough sense by the use of an interpolation function that gradually changes the saturation dependent flow functions according to changes in the mineral composition, see Remark 2 for further motivation.

Previous works. In fact, the model developed in this work represents a proper combination of two models that previously have been proposed, respectively for the study of dynamic wettability alteration [44, 45] and chalk weakening effects due to water-rock interaction [16]. A 1D model for simulation of dynamic wettability alteration in spontaneous imbibition was developed in [44]. See also [43, 23] for similar type of models in the context of low salinity waterflooding on reservoir scale. The model in [44] represents a core plug on laboratory scale where a general wettability alteration (WA) agent is added. The term WA agent is used to represent a single ion or group of ions. In particular, we truncate all the complicated chemical interactions into a single adsorption function. Relative permeability and capillary pressure curves are constructed by employing an interpolation between two sets of generic curves corresponding to oil-wet (mixed wet) and water-wet conditions. Gradually, as the adsorption of the WA agent takes place, there is a shift towards more water-wetness resulting in a corresponding higher oil recovery. The form of the model is as follows (dimensionless form):

$$\begin{aligned} s_t + f(s,c)_x &= \varepsilon([-\lambda_o f](s,c)P_c(s,c)_x)_x \\ (sc + a(c))_t + (cf(s,c))_x &= \delta(D(s)c_x) + \varepsilon(c[-\lambda_o f](s,c)P_c(s,c)_x)_x, \end{aligned} \tag{1}$$

where s is water saturation, c concentration of WA agent, f is fractional flow function, λ_o is oil mobility, P_c capillary pressure, $D(s)$ molecular diffusion coefficient, $a(c)$ adsorption isotherm, whereas ε and δ are dimensionless characteristic numbers. Models of the form (1) have been studied extensively before in connection with for example polymer and surfactant flooding. A nice overview of this activity is given in the book [8] which also includes a comprehensive reference list.

A special feature of the model is that the adsorption process, described by a standard adsorption isotherm (see [44]), makes the rock saturated by the WA agent after some time if there is a steady transport of this agent into the core. This in turn implies that the same wettability change will take place throughout the whole core *independent* of the specific ion concentrations of the brine that is used. It is only a question about how long time this wettability changing process will take. In other words, after an initial transient period, the oil recovery curves will reach the same steady state level. Consequently, such a model cannot be used to explain the experimental results shown in Fig. 1 where different brine compositions give different levels of oil recovery. This observation suggests that a more detailed description of relevant water-rock chemistry should be taken into account.

On the other hand, in [16] a water-rock system was studied for the purpose of describing some recent experimental results where chalk cores were flooded with different brines. A main purpose was to investigate changes in ion concentrations measured at the outlet when cores were flooded with seawater like brines at a temperature $T = 130°\text{C}$. It was observed that the proposed model, which accounted

for combined flow and chemical reactions, could reproduce main trends of the measured ion concentrations at the outlet. A special feature of the model is that different brines give different long-time steady-state type of solutions. A main idea of the present work is to link wettability alteration to this *brine-dependent* steady-state behavior.

Thus, in the current work we adopt this model for the oil-water-ion-mineral system in question. Compared to [16], we have to take into account the water-oil transport mechanisms in an appropriate manner as well as provide a link between the flow functions required for the water-oil transport (relative permeability and capillary pressure) and the water-rock interaction. For that purpose we rely on an approach similar to that used in [44, 43, 23] but where the role played by adsorption of the WA agent now is replaced by dissolution of calcite. This is done by introducing a wettability index $H(\rho_c)$ (lying between 0 and 1) that senses where the dissolution of calcite takes place.

Results. The main contribution of the paper is:

- Formulation of the model that incorporates the essential components required for systematic investigations of the combined effect of two-phase transport mechanisms and water-rock interaction.
- Provide a first evaluation of the model. The 1D model we run is not directly comparable with the setting of most of the experimental results which involve flow in 2D or 3D geometries. However, we are interested in generic features like oil recovery curves as a function of brine composition and/or temperature.

The numerical investigations demonstrate that different oil recovery levels are produced depending on the brine composition. More precisely, for a fixed set of parameters (flow and chemical reaction related parameters) the model predicts increasing oil recovery levels for higher concentration of SO_4^{2-} ions, similarly to the results reflected by Fig. 1 (left). Moreover, the strong enhanced oil recovery effect obtained by increasing the concentration of Mg^{2+} is also captured by the model, see Fig. 1 (right). The model also naturally reflects that temperature plays a crucial role for the resulting oil recovery curve. Consequently, we may conclude that the proposed model demonstrates that the relation between oil recovery curves and brine composition possibly can be understood as a result of the combined effect of transport (molecular diffusion), water-rock interaction in terms of dissolution/precipitation of minerals, and a corresponding wettability alteration due to dissolution of calcite.

The structure of this paper is as follows: In Section 2 we first give a brief overview of the essential ingredients of the model. In Section 3 we describe the equations relevant for the aqueous equilibrium chemistry, as well as non-equilibrium water-rock chemistry (dissolution/precipitation). In Section 4 we describe the saturation dependent flow functions, relative permeability and capillary pressure, typically used for modeling of two-phase transport effects. In particular, we describe an interpolation mechanism that relates dissolution of calcite to a change of the wetting state represented by the relative permeability and capillary pressure functions. The full model where convective and diffusive transport effects are included, together with the water-rock interaction, is described in Section 5. In Section 6 we sketch the numerical approach employed for solving the resulting model (8) and (9), based on an operator splitting approach. Finally, in Section 7 we provide a first evaluation of the model by computing solutions for cases where we change the concentration, respectively, of SO_4^{2-}, Mg^{2+}, and temperature for a seawater like brine.

2. **The model.** In this section we briefly define the oil-water-ion-mineral system we shall work with relevant for spontaneous imbibition lab experiments for chalk core plugs. The details of the derivation of the model are given in Section 3–5. We closely build upon the model that was developed in [16] for the study of a water-ion-rock system. However, compared to that work we now have to consider an extended model where also the oil phase is included. For the modeling of two-phase water-oil transport we follow the approach described in [44], see also references therein.

Let Ω be the domain of calcite $CaCO_3$ and define the molar concentrations of the different species in the units of mol/liter:

$\rho_c = [CaCO_3]$ (solid)	$\rho_{ca} = [Ca^{2+}]$ (ions)	$\rho_h = [H^+]$ (ions)
$\rho_g = [CaSO_4]$ (solid)	$\rho_{mg} = [Mg^{2+}]$ (ions)	$\rho_{oh} = [OH^-]$ (ions)
$\rho_m = [MgCO_3]$ (solid)	$\rho_{so} = [SO_4^{2-}]$ (ions)	$\rho_{hco} = [HCO_3^-]$ (ions)
$\rho_l = [H_2O]$ (water)	$\rho_{na} = [Na^+]$ (ions)	$\rho_{co} = [CO_3^{2-}]$ (ions)
$\rho_o = [\cdot]$ (oil)	$\rho_{cl} = [Cl^-]$ (ions)	

The domain Ω itself may depend on time, due to the undergoing chemical reactions which affect its surface. Currently, we neglect this dependence. Since we are including the bulk volume (matrix volume + pore volume) in the definition of the above densities, we will call them *total concentrations*. Later we shall define *porous concentrations* when dealing with porosity ϕ and volume fraction s for the water phase.

The primary unknown concentrations are ρ_c, ρ_g, ρ_m, ρ_o, ρ_l, ρ_{ca}, ρ_{so}, ρ_{mg}, ρ_{na}, ρ_{cl}, ρ_h, ρ_{oh}, ρ_{co}, and ρ_{hco}. We shall assume that the Na^+ and Cl^- ions do not take part in the chemical reactions, i.e., their concentrations ρ_{na} and ρ_{cl} are determined by the transport mechanisms only. We include chemical kinetics associated with the concentrations ρ_c, ρ_g, ρ_m, ρ_{ca}, ρ_{so}, ρ_{mg} involved in the water-rock interactions (dissolution/precipitation), whereas the concentrations ρ_h, ρ_{oh}, ρ_{co}, and ρ_{hco} involved in the aqueous chemistry, are obtained by considering equilibrium state equations. In addition, a charge balance equation is included for the ions in question.

Water-rock interaction (dissolution and precipitation). The model we shall study represents a reactive transport system with three mineral phases ($CaCO_3$, $CaSO_4$, $MgCO_3$) and three aqueous species (Ca^{2+}, SO_4^{2-}, Mg^{2+}) which react according to basic kinetic laws. More precisely, the chemical reactions we include are:

$$CaCO_3(s) + H^+ \rightleftharpoons Ca^{2+} + HCO_3^- \qquad \text{(dissolution/precipitation)}, \tag{2}$$

$$CaSO_4(s) \rightleftharpoons Ca^{2+} + SO_4^{2-} \qquad \text{(dissolution/precipitation)}, \tag{3}$$

$$MgCO_3(s) + H^+ \rightleftharpoons Mg^{2+} + HCO_3^- \qquad \text{(dissolution/precipitation)}. \tag{4}$$

We shall take into account reaction kinetic relevant for these processes.

Aqueous chemistry (chemical reactions in the water phase). Chemical reactions in the water phase are assumed to be at equilibrium. More precisely, in addition to (2)–(4), we will also make use of the following chemical reactions in order to determine concentrations of HCO_3^-, H^+, CO_3^{2-} and OH^- (which are species

in the water phase):

$$\mathrm{CO_2}(g) + \mathrm{H_2O} \rightleftharpoons \mathrm{HCO_3^-} + \mathrm{H^+}, \tag{5}$$

$$\mathrm{HCO_3^-} \rightleftharpoons \mathrm{CO_3^{2-}} + \mathrm{H^+}, \tag{6}$$

$$\mathrm{H_2O} \rightleftharpoons \mathrm{OH^-} + \mathrm{H^+}. \tag{7}$$

We do not include reaction kinetic associated with these chemical reactions but assume that they are at equilibrium. In other words, it is implicitly assumed that they take place at a much faster time scale than the dissolution/precipitation processes (2)–(4). As mentioned, we shall also include a charge balance equation.

Model for combined water-oil flow and water-rock interaction. The core plug under consideration is initially filled with formation water which is in equilibrium with the minerals inside the pore space. Moreover, initially, the wetting state is assumed to be such that no water will imbibe into the core when it is placed in water.

However, when a brine with ion concentrations different from the formation water is used, there will be a transport of various ions into the core due to molecular diffusion. This creates concentration fronts that move with a certain speed. At these fronts, as well as behind them, chemical reactions will take place, both within the aqueous phase as well as on the rock surface. It is expected that the water-rock interaction then will lead to a change of the wetting state [37, 39, 38, 4, 5, 46, 40, 47]. The model that is formulated should be general enough to explore different hypothesis about possible links between water-rock interaction and changes in the wetting state. However, the main focus of this paper is to build into the model a mechanism that relates wettability alteration (towards a more water-wet state) to dissolution of calcite, see [22] for further motivation.

We follow along the line of previous studies, see for example [1, 2, 3, 9, 10, 44] and references therein, and formulate a one-dimensional model. More precisely, the model we shall deal with takes the following form:

$$\begin{aligned}
(\phi s)_t + \gamma F(s,\rho_c)_x &= \varepsilon (AJ(s,\rho_c)_x)_x,\\
(\phi s C_{na})_t + \gamma (C_{na} F(s,\rho_c))_x &= (DC_{na,x})_x + \varepsilon (C_{na} AJ(s,\rho_c)_x)_x,\\
(\phi s C_{cl})_t + \gamma (C_{cl} F(s,\rho_c))_x &= (DC_{cl,x})_x + \varepsilon (C_{cl} AJ(s,\rho_c)_x)_x,\\
(\phi s C_{ca})_t + \gamma (C_{ca} F(s,\rho_c))_x &= (DC_{ca,x})_x + \varepsilon (C_{ca} AJ(s,\rho_c)_x)_x + \tau(\dot r_c + \dot r_g),\\
(\phi s C_{so})_t + \gamma (C_{so} F(s,\rho_c))_x &= (DC_{so,x})_x + \varepsilon (C_{so} AJ(s,\rho_c)_x)_x + \tau \dot r_g,\\
(\phi s C_{mg})_t + \gamma (C_{mg} F(s,\rho_c))_x &= (DC_{mg,x})_x + \varepsilon (C_{mg} AJ(s,\rho_c)_x)_x + \tau \dot r_m,\\
(\rho_c)_t &= -\tau \dot r_c,\\
(\rho_g)_t &= -\tau \dot r_g,\\
(\rho_m)_t &= -\tau \dot r_m.
\end{aligned} \tag{8}$$

Here γ and ε are dimensionless positive constants, sometimes referred to as, respectively, the gravity number and capillary number. All the details leading to this model are given in the subsequent sections. In the model (8), a characteristic time τ and length scale $L = \sqrt{\overline{D}_m \tau}$ have been introduced. The unknown variables we solve for are water saturation s (dimensionless), and concentrations C_{na}, C_{cl}, C_{ca}, C_{so}, C_{mg}, ρ_c, ρ_g, ρ_m (in terms of mole per liter water). Moreover, $F(s,\rho_c)$ is the fractional flow functions, $D = D(\phi, s)$ the molecular diffusion coefficient, $A = A(s,\rho_c)$ is the coefficient associated with capillary diffusion, and $J(s,\rho_c)$ is the so-called

Leverett function known from the Buckley Leverett theory. The dependence on the calcite concentration ρ_c involved in these functions is due to the proposed coupling between wettability alteration and dissolution of calcite.

In addition, we must specify rate equations $\dot{r}_k = \dot{r}_k(C_{ca}, C_{so}, C_{mg}, C_{na}, C_{cl})$ for $k = c, g, m$. Following [9, 10, 16], and references therein, the reaction terms take the form

$$\begin{aligned}
\dot{r}_c &= k_1^c \Big[\mathrm{sgn}^+(\rho_c) F_c^+(C_{ca}, C_{so}, C_{mg}) - F_c^-(C_{ca}, C_{so}, C_{mg}) \Big], \\
\dot{r}_g &= k_1^g \Big[\mathrm{sgn}^+(\rho_g) F_g^+(C_{ca}, C_{so}, C_{mg}) - F_g^-(C_{ca}, C_{so}, C_{mg}) \Big], \\
\dot{r}_m &= k_1^m \Big[\mathrm{sgn}^+(\rho_m) F_m^+(C_{ca}, C_{so}, C_{mg}) - F_m^-(C_{ca}, C_{so}, C_{mg}) \Big],
\end{aligned} \tag{9}$$

where the functions F_c, F_g, and F_m represent the kinetics of the precipitation and dissolution processes in question and k_1^c, k_1^g, and k_1^m are corresponding reaction rate constants. Here $F_I = F_I^+ - F_I^-$, $I = c, g, m$, is a decomposition of F into its positive and negative parts, whereas $\mathrm{sgn}(x)^+ = 1$ if $x > 0$, otherwise it is 0. $F_I < 0$ represents precipitation, whereas $F_I > 0$ represents dissolution. The above formulation takes into account that a mineral can be dissolved only as long as it exists, and is similar to what has been done in other works, see for example [9, 33] and references therein. C_k represents *porous* concentrations and are related to the total concentrations by $\rho_k = \phi s C_k$, for $k = ca, so, mg, na, cl$.

3. The model for water-rock interaction.

In the following, we first give some more details concerning the equilibrium chemistry associated with the chemical reactions (5)–(7), the aqueous chemistry. Then we describe the relations that take into account kinetics associated with the precipitation/dissolution processes (2)–(4). In particular, we shall distinguish between concentration C and chemical activity a noting that they are related by

$$a = \gamma C, \tag{10}$$

where γ is the activity coefficient. According to the Debuye-Hückel equation, see for example [25, 32], the activity coefficient γ_i is given by

$$-\log_{10}(\gamma_i) = \frac{A Z_i^2 \sqrt{I_0}}{1 + a_i^0 B \sqrt{I_0}}, \tag{11}$$

where the index i refers to the different species involved in the system which is studied. Moreover, Z_i refers to the ionic charges, $A(T)$ and $B(T)$ are temperature dependent given functions [20, 21], similarly for the constants a_i^0, whereas I_0 refers to the ionic strength defined by

$$I_0 = \frac{1}{2} \sum_i C_i Z_i^2. \tag{12}$$

For the numerical calculations, we calculate I_0 based on the ion concentrations for the imbibing brine. Consequently, I_0 is assumed to be constant throughout the imbibition process. Since the temperature is kept constant, the activity coefficients are also taken to be constant, according to (11).

3.1. **Aqueous chemistry.** In the subsequent discussion we assume that we know the concentrations C_{na} and C_{cl}. Based on this we shall discuss the various equations associated with the chemical reactions described by (5)–(7).

We assume that the CO_2 partial pressure P_{CO_2} is known, from which the CO_2 concentration can be determined. More precisely, the local equilibrium associated with (5) gives the relation

$$C_1 = P_{CO_2} K = a_{hco} a_h = (\gamma_{hco}\gamma_h) C_{hco} C_h, \tag{13}$$

for an appropriate choice of the equilibrium constant (solubility product) K and partial pressure P_{CO_2}. The chemical reaction equation (6) gives us

$$C_2 = \frac{a_{co} a_h}{a_{hco}} = \Big(\frac{\gamma_{co}\gamma_h}{\gamma_{hco}}\Big) \frac{C_{co} C_h}{C_{hco}}, \tag{14}$$

where C_2 is a known solubility constant. Moreover, the reaction equation (7) gives

$$C_w = a_h a_{oh} = (\gamma_{oh}\gamma_h) C_{oh} C_h, \tag{15}$$

where C_w is known. The following aqueous charge balance equation is also assumed to hold for the various species contained in the water phase

$$\sum_i C_i Z_i = 0, \tag{16}$$

where Z_i refers to the ionic charge of species i. For the system in question, this results in the following balance equation:

$$2C_{ca} + 2C_{mg} + C_h + C_{na} = 2C_{so} + C_{hco} + 2C_{co} + C_{oh} + C_{cl}. \tag{17}$$

Thus, the four equations (13)–(16) allow us to solve for C_h, C_{hco}, C_{co}, and C_{oh}. This relation can be written in the form

$$C_3 = C_{hco} + 2C_{co} + C_{oh} - C_h, \tag{18}$$

where

$$C_3 = C_3(C_{ca}, C_{mg}, C_{so}; C_{na}, C_{cl}) = 2(C_{ca} + C_{mg} - C_{so}) + (C_{na} - C_{cl}). \tag{19}$$

It's convenient to introduce the following notation:

$$\widetilde{C}_1 = \frac{C_1}{\gamma_{hco}\gamma_h}, \qquad \widetilde{C}_2 = \frac{C_2\gamma_{hco}}{\gamma_{co}\gamma_h}, \qquad \widetilde{C}_w = \frac{C_w}{\gamma_h\gamma_{oh}}. \tag{20}$$

We shall make use of the simplifying assumption that the concentration C_{co} of CO_3^{2-} is relatively low and can be neglected in the charge balance equation (18). Clearly, (18) can then be written in the form

$$C_3 = C_{hco} + \frac{\widetilde{C}_w}{C_h} - C_h, \tag{21}$$

where we have used (15). Combining (13) and (21) we get

$$C_3 = \frac{\widetilde{C}_1 + \widetilde{C}_w}{C_h} - C_h,$$

which results in the second order equation $C_h^2 + C_3 C_h - (\widetilde{C}_1 + \widetilde{C}_w) = 0$. The relevant solution is then given by

$$C_h = \frac{1}{2}\Big(-C_3 + \sqrt{C_3^2 + 4(\widetilde{C}_1 + \widetilde{C}_w)}\Big), \qquad C_{hco} = \frac{\widetilde{C}_1}{C_h}. \tag{22}$$

Finally, C_{co} and C_{oh} can be determined from the equations (14) and (15). In particular, we note that $C_h = C_h(C_{ca}, C_{so}, C_{mg}; C_{na}, C_{cl})$, in view of (19).

3.2. **Rate equations for the water-rock interaction.** The rate equations associated with the water-rock interaction, as described by the dissolution/precipitation processes (2)–(4), are obtained by following an approach similar to that in [9, 16], see also references therein like [25] (chapter 1) and [36, 29]. The main point of this approach is the use of an empirical rate equation of the form

$$R = k(1-\Omega)^n, \tag{23}$$

where R is the rate, k and n are empirical fitting terms and $(1-\Omega)$ the degree of disequilibrium with the mineral in question. Ω is the ratio of the ion activity product (IAP) to the solubility product K for the solid in question, that is, $\Omega = \mathrm{IAP}/K$. If $0 < 1-\Omega$ the solution is undersaturated which may lead to dissolution; if $0 > 1-\Omega$ the solution is supersaturated which implies precipitation.

Thus, the reaction terms $\dot{r}_i$, for $i = c, g, m$ associated with (2)–(4), are given as follows where we have used $n = 1$ in (23):

$$\begin{aligned}
\dot{r}_c &= k_1^c a_c - k_{-1}^c \frac{a_{ca}a_{hco}}{a_h} = k_1^c\Big(1 - \frac{a_{hco}a_{ca}}{K^c a_h}\Big) = k_1^c\Big(1 - \frac{\gamma_{ca}\gamma_{hco}C_{ca}C_{hco}}{\gamma_h C_h K^c}\Big) \\
&= k_1^c\Big(1 - \frac{\gamma_{ca}C_1 C_{ca}}{\gamma_h^2 K^c C_h^2}\Big),
\end{aligned} \tag{24}$$

$$\begin{aligned}
\dot{r}_g &= k_1^g a_g - k_{-1}^g a_{ca}a_{so} = k_1^g\Big(1 - \frac{a_{ca}a_{so}}{K^g}\Big) \\
&= k_1^g\Big(1 - \frac{\gamma_{ca}\gamma_{so}C_{ca}C_{so}}{K^g}\Big),
\end{aligned} \tag{25}$$

$$\begin{aligned}
\dot{r}_m &= k_1^m a_m - k_{-1}^m \frac{a_{mg}a_{hco}}{a_h} = k_1^m\Big(1 - \frac{a_{hco}a_{mg}}{K^m a_h}\Big) = k_1^m\Big(1 - \frac{\gamma_{mg}\gamma_{hco}C_{mg}C_{hco}}{\gamma_h C_h K^m}\Big) \\
&= k_1^m\Big(1 - \frac{\gamma_{mg}C_1 C_{mg}}{\gamma_h^2 K^m C_h^2}\Big),
\end{aligned} \tag{26}$$

where

$$K^c = \frac{k_1^c}{k_{-1}^c}, \qquad K^g = \frac{k_1^g}{k_{-1}^g}, \qquad K^m = \frac{k_1^m}{k_{-1}^m}. \tag{27}$$

Here a_j represents chemical activity associated with species j. Moreover, we have supposed that the minerals exist as pure phases which implies that the ion activities of the minerals are one, see for example [9]. That is, we have set $a_c = a_g = a_m = 1$ in (24)–(26). Mixed phases can be accounted for but that is an unnecessary complication at the present stage. k_{-1}^j represents the rate of precipitation whereas k_1^j represents the rate of dissolution associated with the different species $j = c, g, m$ corresponding to $CaCO_3$, $CaSO_4$, and $MgCO_3$. Similarly, K^j is used to represent the equilibrium constant (solubility product) associated with $j = c, g, m$. These are known values. On the other hand, much less is known about the rate of precipitation/dissolution represented by k_1^j and k_{-1}^j.

It is convenient to introduce the notation

$$\begin{aligned}
F_c(C_{ca}, C_{so}, C_{mg}; C_{na}, C_{cl}) &\overset{\text{def}}{:=} \Big(1 - \frac{\gamma_{ca}\gamma_{hco}C_{ca}C_{hco}}{\gamma_h C_h K^c}\Big), \\
F_g(C_{ca}, C_{so}; C_{na}, C_{cl}) &\overset{\text{def}}{:=} \Big(1 - \frac{\gamma_{ca}\gamma_{so}C_{ca}C_{so}}{K^g}\Big), \\
F_m(C_{ca}, C_{so}, C_{mg}; C_{na}, C_{cl}) &\overset{\text{def}}{:=} \Big(1 - \frac{\gamma_{mg}\gamma_{hco}C_{mg}C_{hco}}{\gamma_h C_h K^m}\Big).
\end{aligned} \tag{28}$$

Then we get the following rate equations associated with the minerals represented by ρ_c, ρ_g, and ρ_m:

$$\begin{aligned}
\frac{d\rho_c}{dt} &= -\dot{r}_c = -k_1^c F_c(C_{ca}, C_{so}, C_{mg}; C_{na}, C_{cl}),\\
\frac{d\rho_g}{dt} &= -\dot{r}_g = -k_1^g F_g(C_{ca}, C_{so}, C_{mg}; C_{na}, C_{cl}),\\
\frac{d\rho_m}{dt} &= -\dot{r}_m = -k_1^m F_m(C_{ca}, C_{so}, C_{mg}; C_{na}, C_{cl}).
\end{aligned} \tag{29}$$

Similarly, (24)–(26) give rise to the following set of rate equations associated with the aqueous species ρ_{ca}, ρ_{so}, and ρ_{mg} involved in the precipitation/dissolution processes (2)–(4):

$$\begin{aligned}
\frac{d\rho_{ca}}{dt} =& \dot{r}_{ca} = \dot{r}_c + \dot{r}_g = k_1^c F_c(C_{ca}, C_{so}, C_{mg}; C_{na}, C_{cl})\\
&+ k_1^g F_g(C_{ca}, C_{so}, C_{mg}; C_{na}, C_{cl}),\\
\frac{d\rho_{so}}{dt} =& \dot{r}_{so} = \dot{r}_g = k_1^g F_g(C_{ca}, C_{so}, C_{mg}; C_{na}, C_{cl}),\\
\frac{d\rho_{mg}}{dt} =& \dot{r}_{mg} = \dot{r}_m = k_1^m F_m(C_{ca}, C_{so}, C_{mg}; C_{na}, C_{cl}).
\end{aligned} \tag{30}$$

An important modification is to take into account the fact that mineral dissolution stops once the mineral has disappeared [9, 16]. To build this mechanism into the rate equations given by (24)–(26), we use (28) and change these equations in the following manner:

$$\begin{aligned}
\dot{r}_c &= k_1^c \Big[\mathrm{sgn}^+(\rho_c) F_c^+(C_{ca}, C_{so}, C_{mg}) - F_c^-(C_{ca}, C_{so}, C_{mg})\Big],\\
\dot{r}_g &= k_1^g \Big[\mathrm{sgn}^+(\rho_g) F_g^+(C_{ca}, C_{so}, C_{mg}) - F_g^-(C_{ca}, C_{so}, C_{mg})\Big],\\
\dot{r}_m &= k_1^m \Big[\mathrm{sgn}^+(\rho_m) F_m^+(C_{ca}, C_{so}, C_{mg}) - F_m^-(C_{ca}, C_{so}, C_{mg})\Big],
\end{aligned} \tag{31}$$

where

$$\mathrm{sgn}^+(x) = \begin{cases} 1, & \text{if } x \geq 0;\\ 0, & \text{otherwise,}\end{cases}$$

$$F_I = F_I^+ - F_I^-, \quad \text{where} \quad F_I^+ = \max(0, F_I), \quad F_I^- = \max(0, -F_I).$$

Clearly, in view of (29), we see that for $F_I < 0$ where $I = c, g, m$ represents the mineral in question, the mineral precipitates; for $F_I = 0$ chemical equilibrium exists and nothing happens; for $F_I > 0$ the mineral dissolves, but only as long as the mineral exists, i.e., $\rho_I > 0$.

4. **Coupling of wettability alteration to changes on the rock surface.** This section discusses aspects concerning the flow functions (relative permeability and capillary pressure) and partially follows ideas employed in previous works [44, 43, 23].

4.1. **Relative permeability and capillary pressure functions.** As a basic model for relative permeability functions the well-known Corey type correlations

are used [15]. They are given in the form (dimensionless functions)

$$\begin{aligned} k(s) &= k^*\Big(\frac{s-s_{wr}}{1-s_{or}-s_{wr}}\Big)^{Nk}, \qquad s_{wr}\le s\le 1-s_{or},\\ k_o(s) &= k_o^*\Big(\frac{1-s_{or}-s}{1-s_{or}-s_{wr}}\Big)^{Nk_o}, \qquad s_{wr}\le s\le 1-s_{or}, \end{aligned} \tag{32}$$

where s_{wr} and s_{or} represent critical saturation values and Nk and Nk_o are the Corey exponents that must be specified. In addition, k^* and k_o^* are the end point relative permeability values that also must be given.

As a simple model for capillary pressure a piecewise linear function of the following form is used:

$$P_c(s) = C^*\begin{cases} 1 & s<s_{wr},\\ 1+\Big(\frac{pc_1-1}{s_1-s_{wr}}\Big)(s-s_{wr}) & s_{wr}\le s\le s_1,\\ pc_1+\Big(\frac{pc_2-pc_1}{s_2-s_1}\Big)(s-s_1) & s_1\le s\le s_2,\\ pc_2+\Big(\frac{-1-pc_2}{1-s_{or}-s_2}\Big)(s-s_2) & s_2\le s\le 1-s_{or},\\ -1 & s>1-s_{or}, \end{cases} \tag{33}$$

where C^* and the points (s_1, pc_1) and (s_2, pc_2) are constants that must be specified. In a more realistic setting these would be based on experimental data and, typically, more than two points would be given. Furthermore, C^* is a scaling constant (characteristic capillary pressure) that contains information about interfacial tension and contact angle effects. More precisely, $P_c(s) = C^*J(s)$, where the dimensionless function $J(s)$ is called the Leverett function and its multiplier C^* takes the form [8, 35, 18]

$$C^* = \frac{\sigma\cos(\theta)}{\sqrt{\kappa/\phi}}, \tag{34}$$

where σ is interfacial tension, θ is contact angle, κ absolute permeability, ϕ porosity. In the following data required to obtain concrete relative permeability and capillary pressure curves are specified that can represent, respectively, oil-wet and water-wet conditions. Note that more precisely, spontaneous imbibition experiments have been carried out for *preferential oil-wet* chalk cores [46, 47] (also referred to as mixed wet conditions) but for simplicity we employ the word "oil-wet".

Oil-wet conditions. The following set of values for *oil-wet* conditions is used:

$$k^{*,ow}=0.7,\ k_o^{*,ow}=0.75,\ s_{wr}^{ow}=0.1,\ s_{or}^{ow}=0.15,\ Nk^{ow}=2,\quad Nk_o^{ow}=3. \tag{35}$$

Applying these values in (32) the following two relative permeability curves are obtained

$$k^{ow}(s; s_{wr}^{ow}, s_{or}^{ow}), \qquad k_o^{ow}(s; s_{wr}^{ow}, s_{or}^{ow}), \qquad \text{for } s_{wr}^{ow}\le s\le 1-s_{or}^{ow}.$$

Similarly, from (33) a corresponding capillary pressure function is obtained

$$P_c^{ow}(s; s_{wr}^{ow}, s_{or}^{ow}), \qquad \text{for } s_{wr}^{ow}\le s\le 1-s_{or}^{ow},$$

where the following values are used

$$(s_1^{ow}, pc_1^{ow}) = (0.2, -0.1), \qquad (s_2^{ow}, pc_2^{ow}) = (0.8, -0.5). \tag{36}$$

Moreover, C^* is associated with a reference capillary pressure value which we denote by $P_{c,r}$

$$C^{*,ow} = P_{c,r}. \tag{37}$$

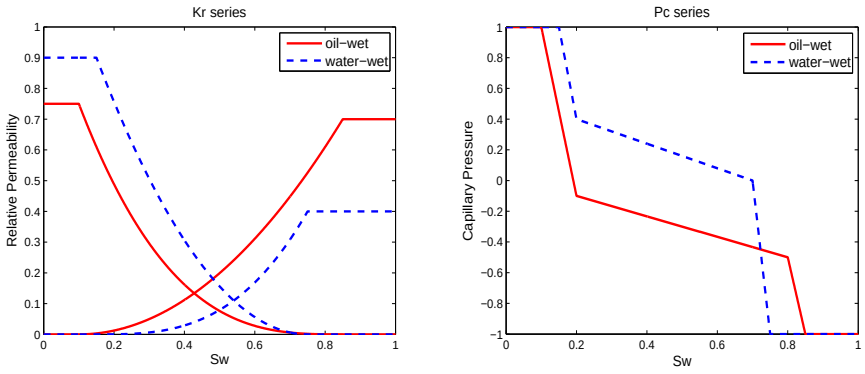

FIGURE 2. **Left**: Example of relative permeability curves corresponding to oil-wet and water-wet conditions. **Right**: Example of capillary pressure curves corresponding to oil-wet and water-wet like conditions.

A specific value for $P_{c,r}$ is given in Section 7. We refer to Fig. 2 for a plot of these curves (red line). For the numerical calculations in Section 7 we shall choose initial water saturation s_{init} such that $P_c^{ow}(s_{\text{init}}) \approx 0$, i.e. $s_{\text{init}} = 0.19$. This implies that no spontaneous imbibition will take place when we start with a core plug that initially is described by P_c^{ow} given by (33) and (36) corresponding to an oil-wet state.

Water-wet conditions. The following set of values for *water-wet* conditions is used:

$$k^{*,ww} = 0.4,\ k_o^{*,ww} = 0.9,\ s_{wr}^{ww} = 0.15,\ s_{or}^{ww} = 0.25,\ Nk^{ww} = 3,\ Nk_o^{ww} = 2. \quad (38)$$

These choices give corresponding relative permeability curves

$$k^{ww}(s; s_{wr}^{ww}, s_{or}^{ww}), \quad k_o^{ww}(s; s_{wr}^{ww}, s_{or}^{ww}), \quad \text{for } s_{wr}^{ww} \le s \le 1 - s_{or}^{ww},$$

and via (33) a corresponding capillary pressure function

$$P_c^{ww}(s; s_{wr}^{ww}, s_{or}^{ww}), \qquad \text{for } s_{wr}^{ww} \le s \le 1 - s_{or}^{ww},$$

with

$$(s_1^{ww}, pc_1^{ww}) = (0.2, 0.4), \qquad (s_2^{ww}, pc_2^{ww}) = (0.7, 0). \quad (39)$$

Again

$$C^{*,ww} = P_{c,r}. \quad (40)$$

We refer to Fig. 2 for a plot of these curves (blue line).

Remark 1. Starting with an initial oil-wet core plug represented by flow functions $P_c = P_c^{ow}$, $k = k^{ow}$, and $k_o = k_o^{ow}$ and an initial saturation s_{init} such that $P_c^{ow}(s_{\text{init}}) = 0$, it's clear that no more oil will come out of the core plug. However, due to molecular diffusion, and the fact that the initial brine in the core plug (formation water) is different from the brine in which the plug is placed, the different ions will move into the core. This creates a non-equilibrium state in the core where the ion concentrations are not in equilibrium with the rock. In particular, this generates chemical reactions in terms of dissolution/precipitation that change the rock surface. In this work we propose to link alteration of the wetting state to these changes in the rock surface.

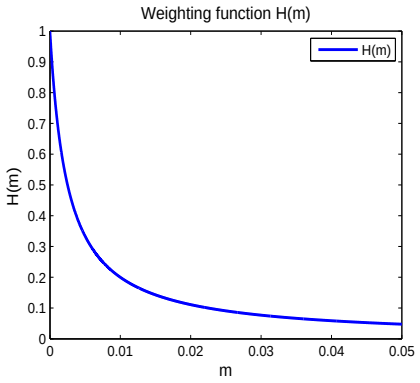

FIGURE 3. The weighting function $H(m)$ as defined by (41) with $r = 400$. The choice of r determines how much calcite that must be dissolved to bring forth a certain change of the wetting state. Note that the function $H(m)$ quickly falls off from 1. This means that the initial dissolution will create a larger wettability alteration. Further dissolution will have less impact on the change of the wetting state.

Different possible links between changes in the mineral composition and alteration of the wetting state is of course possible. The objective of this paper is to explore the hypothesis that dissolution of calcite is a governing force in this process, based on some previous calculations [21, 22]. The implementation of this mechanism in the model is the topic of the subsequent subsection.

4.2. **Dissolution of calcite as a mechanism for wettability alteration.** Having an initial concentration ρ_0 of a mineral with concentration ρ, we define the quantity $m(\rho)$

$$m(\rho) := \max(\rho_0 - \rho, 0)$$

as a measure for the dissolved mineral. Moreover, we define

$$H(\rho) := \frac{1}{1 + rm(\rho)}, \tag{41}$$

where $r > 0$ is a specified constant. In the numerical investigations we use $r = 400$. The function $H(\rho)$ then becomes a weighting function such that

(i) $0 < H(\rho) \leq 1$, for $\rho \geq 0$;
(ii) $H(\rho) = 1$, for $\rho \geq \rho_0$ (no dissolution or precipitation);
(iii) $0 < H(\rho) < 1$ for $\rho < \rho_0$ (dissolution).

How fast $H(\rho)$ is approaching 0 as $m(\rho)$ is increasing, depends on the choice of r. Now, the weighting function $H(\rho)$ can be used to represent the wetting state in the core plug; $H(\rho) = 1$ corresponds to the initial oil-wet state, whereas $H(\rho) \approx 0$ represents the water-wet state. By defining relative permeability and capillary pressure curves by means of the weighting function $H(\rho)$ as described in the next subsection, the model can account for a dynamic change from an initial oil-wet state towards a water-wet state controlled by the degree of dissolution of calcite that takes place inside the core.

Remark 2. The interpolation function $H(\rho)$ defined by (41) represents the average wetting state of the porous media inside a representative elementary volume (REV) [7]. The mathematical form can be motivated by making the following two assumptions:

1. There is a constant number of calcium sites at the pore surface, which is denoted $\Gamma^{\mathrm{T}}_{\mathrm{Ca}}$.
2. The wettability change reaction at the surface is described by the following chemical reaction:

$$>\mathrm{CaR\text{-}COO^0} + \mathrm{X^+} + \mathrm{H_2O} \rightleftharpoons >\mathrm{CaH_2O^+}\,, \tag{42}$$

where $>$ means that the reaction takes place at the surface. $\mathrm{R\text{-}COO^-}$ is an organic ion, and $>\mathrm{CaR\text{-}COO^0}$ is a surface complex consisting of calcium cites at the surface and $>\mathrm{CaH_2O^+}$ and $\mathrm{R\text{-}COO^-}$ ions from the oil phase. Hence, the concentration of $>\mathrm{CaR\text{-}COO^0}$ characterizes the wetting state. In particular, a decrease in the concentration of $>\mathrm{CaR\text{-}COO^0}$ (i.e. higher concentration of $>\mathrm{CaH_2O^+}$) indicates a wettability change towards a more water wet surface. X is a chemical species that facilitates release of organic compounds attached to the surface.

From Assumption 1 above we can write the following equation:

$$\Gamma^{\mathrm{T}}_{\mathrm{Ca}} = \Gamma_{>\mathrm{CaH_2O^+}} + \Gamma_{>\mathrm{CaR\text{-}COO^0}}\,, \tag{43}$$

i.e. the total number of calcium sites is the sum of the concentration of free calcium cites ($\Gamma_{>\mathrm{CaH_2O^+}}$) and the calcium sites with adsorbed organic ions ($\Gamma_{>\mathrm{CaR\text{-}COO^0}}$). Assumption 2 gives the following equilibrium equation:

$$K = \frac{\Gamma_{>\mathrm{CaH_2O^+}}}{\Gamma_{>\mathrm{CaR\text{-}COO^0}}\, m_{\mathrm{X}}}. \tag{44}$$

Here the activity of $\mathrm{H_2O}$ is equal to one and m_{X} is the concentration of X. By combining equation (43) and (44), we get:

$$\Gamma_{>\mathrm{CaR\text{-}COO^0}} = \frac{\Gamma^{\mathrm{T}}_{\mathrm{Ca}}}{1 + m_{\mathrm{X}}\, K}\,. \tag{45}$$

Comparing this equation with equation (41), we find that $H(\rho) = \Gamma_{>\mathrm{CaR\text{-}COO^0}}/\Gamma^{\mathrm{T}}_{\mathrm{Ca}}$ when m_{X} is associated with $m = \max(\rho_0 - \rho, 0)$, and $K = r$. In other words, H coincides with $\Gamma_{>\mathrm{CaR\text{-}COO^0}}$ when it is normalized relatively the total number of calcium sites $\Gamma^{\mathrm{T}}_{\mathrm{Ca}}$. The function $H(\rho)$ falls quite rapidly off from 1 when m increases, see Fig. 3. This indicates that the dissolution will preferentially take place where the oil is adsorbed to the rock surface. In [42] p.162, it is stated that a reaction of the type (42) tends to enhance the dissolution, which could support the proposed functional behavior.

4.3. **Modeling of transition from oil-wet to water-wet conditions.** Improved oil recovery by invasion of seawater in a preferential oil-wet porous medium is ultimately due to changes in various flow parameters. The flow conditions before and after the wettability alteration can be described by capillary pressure curves, relative permeability curves, and residual saturations. In this work wettability alteration is incorporated in these flow parameters by defining capillary pressure $P_c(s, \rho_c)$ and relative permeability curves $k(s, \rho_c), k_o(s, \rho_c)$ through an interpolation between the oil-wet and water-wet curves given in (32)–(40).

More precisely, motivated by the proposed hypothesis that transition from preferential oil-wet towards water-wet conditions depends on the dissolution of $CaCO_3$, the following interpolation is proposed:

$$k(s,\rho_c) = H(\rho_c)k^{ow}(s) + [1 - H(\rho_c)]k^{ww}(s), \tag{46}$$

where $H(\rho_c)$ is defined by (41) and ρ_c is the calcite concentration. Hence, when no dissolution of $CaCO_3$ has taken place it follows that $H(\rho_c) = 1$, implying that $k(s,\rho_c) = k^{ow}(s)$. This reflects the initial preferential oil-wet wetting state. Then, as dissolution of $CaCO_3$ takes place, it follows that $m(\rho_c)$ increases. In particular, if the dissolution effect $m(\rho_c)$ becomes large enough $H(\rho_c) \approx 0$, which means that $k(s,\rho_c) \approx k^{ww}(s)$, reflecting that a wettability alteration has taken place which results in a water-wet wetting state. The same interpolation procedure is natural to use for the capillary pressure curve. That is,

$$P_c(s,\rho_c) = H(\rho_c)P_c^{ow}(s) + [1 - H(\rho_c)]P_c^{ww}(s). \tag{47}$$

Thus, different concentrations of ρ_c below its initial concentration $\rho_{c,0}$ as measured by $m(\rho_c)$, produce capillary pressure curves that lie between the two extremes P_c^{ow} and P_c^{ww}.

5. **The coupled water-oil flow and chemical reaction model.** In a more complete description we also want to take into account convective and diffusive forces associated with the brine as well as the oil phase. In order to include such effects we must consider the following equations for the total concentrations ρ_o, ρ_l, ρ_{ca}, ρ_{so}, ρ_{mg}, ρ_{na}, ρ_{cl}, ρ_c, ρ_g, ρ_m:

$$\begin{aligned}
\partial_t\rho_o + \nabla\cdot(\rho_o\mathbf{v}_o) &= 0, && \text{(oil flowing through the pore space)}\\
\partial_t\rho_l + \nabla\cdot(\rho_l\mathbf{v}_l) &= 0, && \text{(water flowing through the pore space)}\\
\partial_t\rho_{na} + \nabla\cdot(\rho_{na}\mathbf{v}_g) &= 0, && (Na^+\text{-ions in water})\\
\partial_t\rho_{cl} + \nabla\cdot(\rho_{cl}\mathbf{v}_g) &= 0, && (Cl^-\text{-ions in water})\\
\partial_t\rho_{ca} + \nabla\cdot(\rho_{ca}\mathbf{v}_g) &= \dot r_c + \dot r_g, && (Ca^{2+}\text{-ions in water})\\
\partial_t\rho_{so} + \nabla\cdot(\rho_{so}\mathbf{v}_g) &= \dot r_g, && (SO_4^{2-}\text{-ions in water})\\
\partial_t\rho_{mg} + \nabla\cdot(\rho_{mg}\mathbf{v}_g) &= \dot r_m, && (Mg^{2+}\text{-ions in water})\\
\partial_t\rho_c &= -\dot r_c, && (\text{precipitation/dissolution of } CaCO_3)\\
\partial_t\rho_g &= -\dot r_g, && (\text{precipitation/dissolution of } CaSO_4)\\
\partial_t\rho_m &= -\dot r_m, && (\text{precipitation/dissolution of } MgCO_3).
\end{aligned} \tag{48}$$

The first seven equations represent concentrations associated with the pore space, the last three equations are associated with the matrix. Here $\mathbf{v}_o$, $\mathbf{v}_l$ and $\mathbf{v}_g$ are, respectively, the oil, water and species "fluid" velocities. The subsequent derivation of the model closely follows the work [16], however, we now have to account also for the oil phase.

Let s_o denote the oil saturation, i.e. the fraction of volume of the pore space ϕ that is occupied by the oil phase, and s the corresponding water saturation. The two saturations are related by the basic relation $s_o + s = 1$. Furthermore, we define the porous concentration C_o associated with the oil component as the concentration taken with respect to the volume of the pore space occupied by oil and represented by ϕs_o. Hence, C_o and ρ_o are related by

$$\rho_o = \phi s_o C_o. \tag{49}$$

Similarly, the porous concentrations of the various components in the water phase are defined as the concentration taken with respect to the volume of the pores occupied by water ϕs. Consequently, the porous concentrations C_l, C_{na}, C_{cl}, C_{ca}, C_{mg}, and C_{so} are related to the total concentrations by

$$\rho_l = \phi s C_l,\ \rho_{na} = \phi s C_{na},\ \rho_{cl} = \phi s C_{cl},\ \rho_{ca} = \phi s C_{ca},\ \rho_{mg} = \phi s C_{mg},\ \rho_{so} = \phi s C_{so}.$$

Following Aregba-Driollet et al [1, 2, 3], we argue that since oil, water, and the ions in water Na^+, Cl^-, Ca^{2+}, Mg^{2+}, and SO_4^{2-} flow only through the pores of the calcite specimen, the "interstitial" velocity $\mathbf{v}_o$ associated with the oil, $\mathbf{v}_l$ associated with the water, and $\mathbf{v}_g$ associated with the ions, have to be defined with respect to the concentrations inside the pores, and differ from the respective seepage velocities $\mathbf{V}_o$, $\mathbf{V}_l$ and $\mathbf{V}_g$. The velocities are related by the Dupuit-Forchheimer relations, see [2] and references therein,

$$\mathbf{V}_o = \phi s_o \mathbf{v}_o, \qquad \mathbf{V}_l = \phi s \mathbf{v}_l, \qquad \mathbf{V}_g = \phi s \mathbf{v}_g. \tag{50}$$

Consequently, the balance equations (48) can be written in the form

$$\begin{aligned}
\partial_t(\phi s_o C_o) + \nabla\cdot(C_o \mathbf{V}_o) &= 0,\\
\partial_t(\phi s C_l) + \nabla\cdot(C_l \mathbf{V}_l) &= 0,\\
\partial_t(\phi s C_{na}) + \nabla\cdot(C_{na} \mathbf{V}_g) &= 0,\\
\partial_t(\phi s C_{cl}) + \nabla\cdot(C_{cl} \mathbf{V}_g) &= 0,\\
\partial_t(\phi s C_{ca}) + \nabla\cdot(C_{ca} \mathbf{V}_g) &= \dot r_c + \dot r_g,\\
\partial_t(\phi s C_{so}) + \nabla\cdot(C_{so} \mathbf{V}_g) &= \dot r_g,\\
\partial_t(\phi s C_{mg}) + \nabla\cdot(C_{mg} \mathbf{V}_g) &= \dot r_m,\\
\partial_t \rho_c &= -\dot r_c,\\
\partial_t \rho_g &= -\dot r_g,\\
\partial_t \rho_m &= -\dot r_m.
\end{aligned} \tag{51}$$

In order to close the system we must determine the seepage velocities $\mathbf{V}_o$, $\mathbf{V}_l$ and $\mathbf{V}_g$. For that purpose we consider the concentration of the water phase (brine) C that occupies the pore space as a mixture of water C_l and the various species Na^+, Cl^-, Ca^{2+}, Mg^{2+}, and SO_4^{2-} represented by C_g. In other words,

$$C_g = C_{na} + C_{cl} + C_{ca} + C_{mg} + C_{so}, \qquad C = C_g + C_l. \tag{52}$$

Then, we define the seepage velocity $\mathbf{V}$ associated with C by

$$C\mathbf{V} := C_g \mathbf{V}_g + C_l \mathbf{V}_l. \tag{53}$$

Now we are in a position to rewrite the model in terms of $\mathbf{V}$ and the diffusive velocity $\mathbf{U}_g$ given by

$$\mathbf{U}_g = \mathbf{V}_g - \mathbf{V}. \tag{54}$$

Then the model (51) takes the form

$$\begin{aligned}
\partial_t(\phi s_o C_o) + \nabla\cdot(C_o\mathbf{V}_o) &= 0,\\
\partial_t(\phi s C_l) + \nabla\cdot(C_l\mathbf{V}_l) &= 0,\\
\partial_t(\phi s C_{na}) + \nabla\cdot(C_{na}\mathbf{U}_g) &= -\nabla\cdot(C_{na}\mathbf{V}),\\
\partial_t(\phi s C_{cl}) + \nabla\cdot(C_{cl}\mathbf{U}_g) &= -\nabla\cdot(C_{cl}\mathbf{V}),\\
\partial_t(\phi s C_{ca}) + \nabla\cdot(C_{ca}\mathbf{U}_g) &= (\dot r_c + \dot r_g) - \nabla\cdot(C_{ca}\mathbf{V}),\\
\partial_t(\phi s C_{so}) + \nabla\cdot(C_{so}\mathbf{U}_g) &= \dot r_g - \nabla\cdot(C_{so}\mathbf{V}),\\
\partial_t(\phi s C_{mg}) + \nabla\cdot(C_{mg}\mathbf{U}_g) &= \dot r_m - \nabla\cdot(C_{mg}\mathbf{V}),\\
\partial_t\rho_c &= -\dot r_c,\\
\partial_t\rho_g &= -\dot r_g,\\
\partial_t\rho_m &= -\dot r_m.
\end{aligned} \tag{55}$$

Furthermore, we can assume that the seepage velocity $\mathbf{V}$ associated with the water phase represented by C, is given by Darcy's law [2, 6, 30]

$$\mathbf{V} = -\kappa\lambda(\nabla p - \rho g\nabla d), \qquad \lambda = \frac{k}{\mu} \tag{56}$$

where κ is permeability and μ is viscosity, and p pressure in water phase. Similarly, for the oil phase

$$\mathbf{V}_o = -\kappa\lambda_o(\nabla p_o - \rho_o g\nabla d), \qquad \lambda_o = \frac{k_o}{\mu_o} \tag{57}$$

The diffusive velocity $\mathbf{U}_g$ is expressed by Fick's law by

$$C_\alpha\mathbf{U}_g = -D\nabla C_\alpha, \qquad \alpha = na, cl, ca, so, mg, \qquad D = (\phi^p s^q D_m + \alpha|\mathbf{V}|)I, \tag{58}$$

where D_m is the effective molecular diffusion coefficient, α is the dispersion length (longitudinal and transversal dispersion lengths are here taken to be equal), and I is the identity tensor. In view of (52) and (58), it follows that

$$C_g\mathbf{U}_g = -D\nabla C_g. \tag{59}$$

Note that we assume that the diffusion coefficient D is the same for all species $\alpha = na, cl, ca, so, mg$. This is a reasonable assumption as long as the concentration is not too high, see e.g. [9]. Moreover, we shall apply the following simplified molecular diffusion coefficient (based on Archie's law)

$$D = D_m\phi^p s^q I, \qquad 1 \le p, q \le 2.5, \tag{60}$$

where the mechanical dispersion term is neglected since we focus on spontaneous imbibition. The coefficient p is referred to as the cementation exponent, q as the saturation exponent. The cementation exponent is often close to 2 whereas the saturation exponent is also often fixed at a value in the same range, see for example [11, 14, 7]. For the simulations we have used $p = q = 1.9$. Using (58) and (60) in

(55) yields

$$\begin{aligned}
\partial_t(\phi s_o C_o) + \nabla\cdot(C_o\mathbf{V}_o) &= 0,\\
\partial_t(\phi s C_l) + \nabla\cdot(C_l\mathbf{V}_l) &= 0,\\
\partial_t(\phi s C_{na}) - \nabla\cdot(D\nabla C_{na}) &= -\nabla\cdot(C_{na}\mathbf{V}),\\
\partial_t(\phi s C_{cl}) - \nabla\cdot(D\nabla C_{cl}) &= -\nabla\cdot(C_{cl}\mathbf{V}),\\
\partial_t(\phi s C_{ca}) - \nabla\cdot(D\nabla C_{ca}) &= (\dot r_c + \dot r_g) - \nabla\cdot(C_{ca}\mathbf{V}),\\
\partial_t(\phi s C_{so}) - \nabla\cdot(D\nabla C_{so}) &= \dot r_g - \nabla\cdot(C_{so}\mathbf{V}),\\
\partial_t(\phi s C_{mg}) - \nabla\cdot(D\nabla C_{mg}) &= \dot r_m - \nabla\cdot(C_{mg}\mathbf{V}),\\
\partial_t\rho_c &= -\dot r_c,\\
\partial_t\rho_g &= -\dot r_g,\\
\partial_t\rho_m &= -\dot r_m.
\end{aligned} \tag{61}$$

In particular, summing the equations corresponding to C_{na}, C_{cl}, C_{ca}, C_{so}, and C_{mg}, we obtain an equation for C_g in the form

$$\partial_t(\phi s C_g) - \nabla\cdot(D\nabla C_g) = (\dot r_c + 2\dot r_g + \dot r_m) - \nabla\cdot(C_g\mathbf{V}). \tag{62}$$

In a similar manner, using $C_l\mathbf{V}_l = C_l\mathbf{V} - C_g\mathbf{U}_g$ (obtained from (53), (54), and (52)) in the second equation of (61), the following equation is obtained

$$\partial_t(\phi s C_l) + \nabla\cdot(C_l\mathbf{V}) = \nabla\cdot(C_g\mathbf{U}_g). \tag{63}$$

Summing (63) and (62), we get the following equation for the concentration of the water phase with its different chemical components, represented by $C = C_g + C_l$,

$$\partial_t(\phi s C) + \nabla\cdot(C\mathbf{V}) = (\dot r_c + 2\dot r_g + \dot r_m). \tag{64}$$

To sum up, we have a model in the form

$$\begin{aligned}
\partial_t(\phi s_o C_o) + \nabla\cdot(C_o\mathbf{V}_o) &= 0,\\
\partial_t(\phi s C) + \nabla\cdot(C\mathbf{V}) &= (\dot r_c + 2\dot r_g + \dot r_m),\\
\partial_t(\phi s C_{na}) + \nabla\cdot(C_{na}\mathbf{V}) &= \nabla\cdot(D\nabla C_{na}),\\
\partial_t(\phi s C_{cl}) + \nabla\cdot(C_{cl}\mathbf{V}) &= \nabla\cdot(D\nabla C_{cl}),\\
\partial_t(\phi s C_{ca}) + \nabla\cdot(C_{ca}\mathbf{V}) &= \nabla\cdot(D\nabla C_{ca}) + (\dot r_c + \dot r_g),\\
\partial_t(\phi s C_{so}) + \nabla\cdot(C_{so}\mathbf{V}) &= \nabla\cdot(D\nabla C_{so}) + \dot r_g,\\
\partial_t(\phi s C_{mg}) + \nabla\cdot(C_{mg}\mathbf{V}) &= \nabla\cdot(D\nabla C_{mg}) + \dot r_m,\\
\partial_t\rho_c &= -\dot r_c,\\
\partial_t\rho_g &= -\dot r_g,\\
\partial_t\rho_m &= -\dot r_m,
\end{aligned} \tag{65}$$

where $D = D(\phi, s)$ as given by (60).

Simplifying assumptions. Before we proceed some simplifying assumptions are made:

- The oil and water component densities C_o and C are assumed to be constant, i.e., incompressible fluids;
- The effect from the chemical reactions in the water phase equation (second equation of (65)) is neglected which is reasonable since the concentration of the water phase C is much larger than the concentrations of the ion exchange

involved in the chemical reactions, this is consistent with [16]. See [2, 3] for an air-rock system where this effect is not neglected;
- Constant porosity ϕ, absolute permeability κ, viscosities μ, μ_o;
- One dimensional flow in a vertical domain.

This results in the following simplified model where h is used to represent the spatial coordinate:

$$\begin{aligned}
\partial_t(\phi s_o) + \partial_h(V_o) &= 0,\\
\partial_t(\phi s) + \partial_h(V) &= 0,\\
\partial_t(\phi s C_{na}) + \partial_h(C_{na}V) &= \partial_h(D(\phi,s)\partial_h C_{na}),\\
\partial_t(\phi s C_{cl}) + \partial_h(C_{cl}V) &= \partial_h(D(\phi,s)\partial_h C_{cl}),\\
\partial_t(\phi s C_{ca}) + \partial_h(C_{ca}V) &= \partial_h(D(\phi,s)\partial_h C_{ca}) + (\dot r_c + \dot r_g),\\
\partial_t(\phi s C_{so}) + \partial_h(C_{so}V) &= \partial_h(D(\phi,s)\partial_h C_{so}) + \dot r_g,\\
\partial_t(\phi s C_{mg}) + \partial_h(C_{mg}V) &= \partial_h(D(\phi,s)\partial_h C_{mg}) + \dot r_m,\\
\partial_t \rho_c &= -\dot r_c,\\
\partial_t \rho_g &= -\dot r_g,\\
\partial_t \rho_m &= -\dot r_m,
\end{aligned} \tag{66}$$

In view of (56) and (57) in a vertical 1D domain, we get

$$V = -\kappa\lambda[(p)_h - \rho g], \qquad \lambda(s,\rho_c) = \frac{k(s,\rho_c)}{\mu} \tag{67}$$

$$V_o = -\kappa\lambda_o[(p_o)_h - \rho_o g], \qquad \lambda_o(s,\rho_c) = \frac{k_o(s,\rho_c)}{\mu_o}, \tag{68}$$

Here g is the gravity constant $g = 9.81$. Moreover, capillary pressure $P_c(s,\rho_c)$ is defined as the difference between oil and water pressure

$$P_c(s,\rho_c) = p_o - p, \tag{69}$$

where P_c is a known function. Total velocity v_T is given by

$$\begin{aligned}
v_T := V + V_o &= -\kappa\Big(\lambda[p_h - \rho g] + \lambda_o[(p_o)_h - \rho_o g]\Big)\\
&= -\kappa\Big(\lambda[(p_o)_h - (P_c)_h - \rho g] + \lambda_o[(p_o)_h - \rho_o g]\Big)\\
&= -\kappa\Big(\lambda_T(p_o)_h - \lambda(P_c)_h - g[\lambda\rho + \lambda_o\rho_o]\Big)\\
&= -\kappa\lambda_T(p_o)_h + \kappa\lambda(P_c)_h + \kappa g[\lambda\rho + \lambda_o\rho_o],
\end{aligned} \tag{70}$$

where total mobility λ_T

$$\lambda_T = \lambda + \lambda_o, \tag{71}$$

has been introduced. Summing the two first equations of (66) and using that $1 = s + s_o$, implies that $(v_T)_h = 0$, i.e., v_T =constant and is determined, for example, from the boundary conditions. From (70) it follows that

$$p_o = \int^h \frac{1}{\lambda_T}\Big(\lambda(P_c)_h + g[\lambda\rho + \lambda_o\rho_o] - \frac{v_T}{\kappa}\Big)\,dh, \tag{72}$$

which can be used to obtain p_o once s and ρ_c are known. From the continuity equation for s given by the second equation of (66) it follows (since $V = -\kappa\lambda[(p_o)_h -$

$(P_c)_h - \rho g])$

$$(\phi s)_t + \Big(-\kappa\lambda(p_o)_h\Big)_h + \Big(\kappa\lambda(P_c)_h\Big)_h + \Big(\kappa\lambda\rho g\Big)_h = 0, \tag{73}$$

where, in view of (70),

$$-\kappa(p_o)_h = \frac{v_T}{\lambda_T} - \kappa\frac{\lambda}{\lambda_T}(P_c)_h - \kappa g[\frac{\lambda}{\lambda_T}\rho + \frac{\lambda_o}{\lambda_T}\rho_o].$$

Thus,

$$\begin{aligned}(\phi s)_t + \Big(\lambda\Big[\frac{v_T}{\lambda_T} - \kappa\frac{\lambda}{\lambda_T}(P_c)_h - \kappa g[\frac{\lambda}{\lambda_T}\rho + \frac{\lambda_o}{\lambda_T}\rho_o]\Big]\Big)_h \\ + \Big(\kappa\lambda(P_c)_h\Big)_h + \Big(\kappa\lambda\rho g\Big)_h = 0.\end{aligned} \tag{74}$$

The fractional flow function $f(s,\rho_c)$ and $f_o(s,\rho_c)$ are defined as follows

$$f(s,\rho_c) \stackrel{\text{def}}{:=} \frac{\lambda(s,\rho_c)}{\lambda(s,\rho_c)+\lambda_o(s,\rho_c)}, \tag{75}$$

$$f_o(s,\rho_c) \stackrel{\text{def}}{:=} \frac{\lambda_o(s,\rho_c)}{\lambda(s,\rho_c)+\lambda_o(s,\rho_c)} = 1 - f(s,\rho_c). \tag{76}$$

Using this in (74) implies that

$$(\phi s)_t + \Big(v_T f(s,\rho_c) + \kappa g\Delta\rho[f\lambda_0](s,\rho_c)\Big)_h - \Big(\kappa[\lambda f](s,\rho_c)(P_c)_h - \kappa\lambda(s,\rho_c)(P_c)_h\Big)_h = 0, \tag{77}$$

where $\Delta\rho = [\rho - \rho_o]$. Noting from (75) that $\lambda f - \lambda = -\lambda_o f$, (77) can be written in the form

$$(\phi s)_t + \Big(v_T f(s,\rho_c) + \Delta\rho\kappa g[f\lambda_0](s,\rho_c)\Big)_h = -\Big(\kappa[\lambda_o f](s,\rho_c)(P_c(s,\rho_c))_h\Big)_h. \tag{78}$$

The same procedure can be applied for the continuity equation for the different ions in water in (66). This gives the following equation for $i = na, cl, ca, so, mg$:

$$\begin{aligned}(\phi s C_i)_t + \Big(C_i\Big[v_T f(s,\rho_c) + \Delta\rho\kappa g[f\lambda_0](s,\rho_c)\Big]\Big)_h \\ = (D(s)C_{i,h})_h - \Big(\kappa C_i[\lambda_o f](s,\rho_c)(P_c(s,\rho_c))_h\Big)_h + \text{Reaction}_i,\end{aligned} \tag{79}$$

Thus, in view of (78) and (79), a model has been obtained of the form

$$\begin{aligned}
\partial_t(\phi s) + \partial_h F(s,\rho_c) &= \partial_h(A(s,\rho_c)\partial_h P_c(s,\rho_c)), \\
\partial_t(\phi s C_{na}) + \partial_h(C_{na}F(s,\rho_c)) &= \partial_h(D\partial_h C_{na}) + \partial_h(C_{na}A(s,\rho_c)\partial_h P_c(s,\rho_c)), \\
\partial_t(\phi s C_{cl}) + \partial_h(C_{cl}F(s,\rho_c)) &= \partial_h(D\partial_h C_{cl}) + \partial_h(C_{cl}A(s,\rho_c)\partial_h P_c(s,\rho_c)), \\
\partial_t(\phi s C_{ca}) + \partial_h(C_{ca}F(s,\rho_c)) &= \partial_h(D\partial_h C_{ca}) + \partial_h(C_{ca}A(s,\rho_c)\partial_h P_c(s,\rho_c)) \\
&\quad + (\dot r_c + \dot r_g), \\
\partial_t(\phi s C_{so}) + \partial_h(C_{so}F(s,\rho_c)) &= \partial_h(D\partial_h C_{so}) + \partial_h(C_{so}A(s,\rho_c)\partial_h P_c(s,\rho_c)) + \dot r_g, \\
\partial_t(\phi s C_{mg}) + \partial_h(C_{mg}F(s,\rho_c)) &= \partial_h(D\partial_h C_{mg}) + \partial_h(C_{mg}A(s,\rho_c)\partial_h P_c(s,\rho_c)) + \dot r_m, \\
\partial_t\rho_c &= -\dot r_c, \\
\partial_t\rho_g &= -\dot r_g, \\
\partial_t\rho_m &= -\dot r_m,
\end{aligned} \tag{80}$$

$$\text{where} \quad \begin{aligned} &F(s,\rho_c) = v_T f(s,\rho_c) + g\Delta\rho\kappa G(s,\rho_c), \qquad G(s,\rho_c) = [f\lambda_o](s,\rho_c) \\ &A(s,\rho_c) = -\kappa G(s,\rho_c). \end{aligned} \tag{81}$$

Counter-current flow. In the following we shall assume that the two-phase flow takes place as *counter-current flow*, i.e., the total velocity v_T is zero inside the core, $v_T = 0$. This assumption is reasonable in light of the fact that the experiments we want to simulate involve spontaneous imbibition in a 1D domain where the main driving force is capillary diffusion. Implicitly, it is assumed that when water imbibes the advancing water displaces from the pore space an equal volume of oil, which flows back to the surface of the block and escapes through the inlet. Thus, capillarity causes equal and opposite flows of the fluids, and this process is referred to as counter-current imbibition. In that respect our model bears similarities to the two-phase model studied by Silin and Patzek [35] where focus is on countercurrent imbibition when the relaxation time is allowed to be saturation dependent. See also [18, 34] for similar studies. Note however, that in a higher dimensional setting the assumption that $V_T = 0$ may not be true [35].

Scaled version of the model. First, we introduce the variables

$$\begin{aligned} &b := \phi s C_{na} = \rho_{na}, \qquad c := \phi s C_{cl} = \rho_{cl}, \\ &x := \phi s C_{ca} = \rho_{ca}, \qquad y := \phi s C_{so} = \rho_{so}, \qquad z := \phi s C_{mg} = \rho_{mg}, \\ &u := \rho_c, \qquad v := \rho_g, \qquad w := \rho_m. \end{aligned} \tag{82}$$

Let τ (sec) be the time scale of the problem. Then, an appropriate space scale could be given by the diffusive typical length L (m)

$$L = \sqrt{\overline{D}_m \tau}, \tag{83}$$

where $\overline{D}_m$ (m^2/s) is a reference diffusion coefficient. We then define dimensionless space h' and time t' variables as follows

$$h' = \frac{h}{\sqrt{\overline{D}_m \tau}}, \qquad t' = \frac{t}{\tau}. \tag{84}$$

We introduce reference viscosity $\overline{\mu}$ (Pa s) and capillary pressure $\overline{P_c} = C^*$ (Pa). Then we define dimensionless coefficients

$$D'_m = \frac{D_m}{\overline{D}_m}, \qquad \mu' = \frac{\mu}{\overline{\mu}}, \qquad P'_c = \frac{P_c}{\overline{P_c}} = J, \qquad \lambda'_o = \frac{k_o}{\mu'_o}. \tag{85}$$

Rewriting (80) in terms of the dimensionless space and time variables (84) and using (85), the following form of the system is obtained (skipping the prime notation)

$$
\begin{aligned}
\partial_t(\phi s) + \gamma\partial_h F(s,u) =& \varepsilon\partial_h(A(s,u)\partial_h J(s,u)), \qquad (86)\\
\partial_t(b) + \gamma\partial_h(C_{na}F(s,u)) =& \delta\partial_h(\phi^p s^q \partial_h C_{na}) + \varepsilon\partial_h(C_{na}A(s,u)\partial_h J(s,u)),\\
\partial_t(c) + \gamma\partial_h(C_{cl}F(s,u)) =& \delta\partial_h(\phi^p s^q \partial_h C_{cl}) + \varepsilon\partial_h(C_{cl}A(s,u)\partial_h J(s,u)),\\
\partial_t(x) + \gamma\partial_h(C_{ca}F(s,u)) =& \delta\partial_h(\phi^p s^q \partial_h C_{ca}) + \varepsilon\partial_h(C_{ca}A(s,u)\partial_h J(s,u))\\
&+ \tau(\dot r_c + \dot r_g),\\
\partial_t(y) + \gamma\partial_h(C_{so}F(s,u)) =& \delta\partial_h(\phi^p s^q \partial_h C_{so}) + \varepsilon\partial_h(C_{so}A(s,u)\partial_h J(s,u)) + \tau\dot r_g,\\
\partial_t(z) + \gamma\partial_h(C_{mg}F(s,u)) =& \delta\partial_h(\phi^p s^q \partial_h C_{mg}) + \varepsilon\partial_h(C_{mg}A(s,u)\partial_h J(s,u)) + \tau\dot r_m, \qquad (87)
\end{aligned}
$$

$$
\begin{aligned}
\partial_t u =& -\tau\dot r_c,\\
\partial_t v =& -\tau\dot r_g, \qquad (88)\\
\partial_t w =& -\tau\dot r_m,
\end{aligned}
$$

with

$$
F(s,u) = [f\lambda_o](s,u), \qquad A(s,u) = -[f\lambda_o](s,u), \qquad (89)
$$

and where the dimensionless characteristic numbers γ and ε, sometimes referred to as, respectively, the *gravity number* and the *capillary number*, are given by

$$
\gamma = \frac{L\Delta\rho\kappa g}{\overline{\mu}\overline{D_m}}, \qquad \varepsilon = \frac{\kappa\overline{P_c}}{\overline{\mu}\overline{D_m}}, \qquad \delta = D_m. \qquad (90)
$$

We choose $\overline{D}_m = D_m$ in (85) such that $D'_m = 1$ and $\delta = 1$.

5.1. **Boundary and initial conditions.** In order to have a well defined system to solve we must specify appropriate initial and boundary conditions.

Boundary conditions. Both ends of the core are exposed to a brine with specified concentrations of the various species, hence, it is natural to use the Dirichlet condition

$$
s(0^-,t) = s(1^+,t) = 1.0, \qquad C_i(0^-,t) = C_i(1^+,t) = C_i^*, \qquad (91)
$$

for the species $i = na, cl, ca, so, mg$ where C_i^* is the specified ion concentrations of the brine that is used. In addition, we also have the boundary condition that capillary pressure is zero outside the core, i.e.

$$
J(t)|_{h=0^-} = J(t)|_{h=1^+} = 0, \qquad (92)
$$

which implies that the capillary diffusion term causes imbibition of the brine into the core plug only if $J(s,u)|_{h=0^+} > 0$ and/or $J(s,u)|_{h=1^-} > 0$. Concerning the equations (87) for the concentrations C_i, it is assumed that molecular diffusion is the only force that makes the species enter at the top and bottom surface. In other words, we use the condition that

$$
\gamma[C_i F(s,u)] - \varepsilon[C_i A(s,u)\partial_h J(s,u)] = 0, \qquad \text{for } h = 0, 1. \qquad (93)
$$

Initial data. Initially, the plug is filled with oil and 19.1% formation water and it is placed in the given brine. Thus, initial data are given by

$$s|_{t=0}(h) = s_{\text{init}} = 0.191, \qquad h \in [0,1],$$

and for $i = na, cl, ca, so, mg$,

$$\begin{aligned} &C_i|_{t=0}(h) = C_{i,0}, \\ &u|_{t=0}(h) = u_0, \quad v|_{t=0}(h) = v_0, \quad w|_{t=0}(h) = w_0, \qquad h \in [0,1], \end{aligned} \tag{94}$$

for given initial concentration of the species $C_{i,0}$ in the water phase and given initial mineral concentrations u_0, v_0, and w_0.

6. Discrete approximations.

6.1. Numerical discretization.

Let us introduce $\mathbf{U} = (u, v, w)^T$ and $\mathbf{C} = (\phi s, b, c, x, y, z)^T$. We assume that we have approximate solutions $(\mathbf{U}^n(\cdot), \mathbf{C}^n(\cdot)) \approx (\mathbf{U}(\cdot, t^n), \mathbf{C}(\cdot, t^n))$. Now, we want to calculate an approximation at the next time level $(\mathbf{U}^{n+1}(\cdot), \mathbf{C}^{n+1}(\cdot)) \approx (\mathbf{U}(\cdot, t^{n+1}), \mathbf{C}(\cdot, t^{n+1}))$ by using a two-step operator splitting approach [26, 17].

Step 1: Chemical reactions. Let S_t be the operator associated with the solution of the following system of ODEs:

$$\begin{aligned} \frac{d(\phi s)}{dt} &= 0, \\ \frac{d(\phi s C_{na})}{dt} &= 0, \\ \frac{d(\phi s C_{cl})}{dt} &= 0, \\ \frac{d(\phi s C_{ca})}{dt} &= A_1^c \Big[\text{sgn}^+(u) F_c^+(C_{ca}, C_{so}, C_{mg}) - F_c^-(C_{ca}, C_{so}, C_{mg}) \Big] \\ &\quad + A_1^g \Big[\text{sgn}^+(v) F_g^+(C_{ca}, C_{so}, C_{mg}) - F_g^-(C_{ca}, C_{so}, C_{mg}) \Big], \\ \frac{d(\phi s C_{so})}{dt} &= A_1^g \Big[\text{sgn}^+(v) F_g^+(C_{ca}, C_{so}, C_{mg}) - F_g^-(C_{ca}, C_{so}, C_{mg}) \Big], \\ \frac{d(\phi s C_{mg})}{dt} &= A_1^m \Big[\text{sgn}^+(w) F_m^+(C_{ca}, C_{so}, C_{mg}) - F_m^-(C_{ca}, C_{so}, C_{mg}) \Big], \\ \frac{du}{dt} &= -A_1^c \Big[\text{sgn}^+(u) F_c^+(C_{ca}, C_{so}, C_{mg}) - F_c^-(C_{ca}, C_{so}, C_{mg}) \Big], \\ \frac{dv}{dt} &= -A_1^g \Big[\text{sgn}^+(v) F_g^+(C_{ca}, C_{so}, C_{mg}) - F_g^-(C_{ca}, C_{so}, C_{mg}) \Big], \\ \frac{dw}{dt} &= -A_1^m \Big[\text{sgn}^+(w) F_m^+(C_{ca}, C_{so}, C_{mg}) - F_m^-(C_{ca}, C_{so}, C_{mg}) \Big], \end{aligned} \tag{95}$$

where $A_1^I = \tau k_1^I$, for $I = c, g, m$. Here F_I is given by (28). Note also that F_I depends on C_{na} and C_{cl}, however, these appear as constants in the ODE system (95) and are therefore not explicitly expressed. Thus, we solve a model of the following form

$$\begin{aligned} \frac{d\mathbf{C}}{dt} &= \mathbf{F}(\mathbf{U}, \mathbf{C}), \qquad \frac{d\mathbf{U}}{dt} = \mathbf{G}(\mathbf{U}, \mathbf{C}), \qquad t \in (0, \Delta t], \\ \mathbf{C}(\cdot, 0) &= \mathbf{C}^n(\cdot), \qquad \mathbf{U}(\cdot, 0) = \mathbf{U}^n(\cdot). \end{aligned} \tag{96}$$

Note that this system corresponds to solving

$$\begin{aligned}\frac{dC_{ca}}{dt} &= \frac{A_1^c}{(\phi s)}\Big[\mathrm{sgn}^+(u)F_c^+(C_{ca},C_{so},C_{mg}) - F_c^-(C_{ca},C_{so},C_{mg})\Big] \\ &\quad + \frac{A_1^g}{(\phi s)}\Big[\mathrm{sgn}^+(v)F_g^+(C_{ca},C_{so},C_{mg}) - F_g^-(C_{ca},C_{so},C_{mg})\Big], \\ \frac{dC_{so}}{dt} &= \frac{A_1^g}{(\phi s)}\Big[\mathrm{sgn}^+(v)F_g^+(C_{ca},C_{so},C_{mg}) - F_g^-(C_{ca},C_{so},C_{mg})\Big], \\ \frac{dC_{mg}}{dt} &= \frac{A_1^m}{(\phi s)}\Big[\mathrm{sgn}^+(w)F_m^+(C_{ca},C_{so},C_{mg}) - F_m^-(C_{ca},C_{so},C_{mg})\Big],\end{aligned} \tag{97}$$

where

$$\begin{aligned}u(t) &= u_0 - (x-y)(t) + (x_0 - y_0), \\ v(t) &= v_0 - y(t) + y_0, \\ w(t) &= w_0 - z(t) + z_0,\end{aligned} \tag{98}$$

for

$$x = \phi s C_{ca}, \qquad y = \phi s C_{so}, \qquad z = \phi s C_{mg}.$$

From this we obtain intermediate approximations $(\mathbf{C}^{n+1/2}, \mathbf{U}^{n+1/2}) = S_{\Delta t}(\mathbf{C}^n, \mathbf{U}^n)$. The stiff ODE system given by (97)and (98) is in this work solved by using the Matlab function ode23 [16].

Step 2: Convection and Diffusion. Let D_t be the operator associated with the solution of the following system of parabolic PDEs:

$$\begin{aligned}\partial_t(\phi s) + \gamma\partial_h F(s,u) &= \varepsilon\partial_h(A(s,u)\partial_h J(s,u)), \\ \partial_t(b) + \gamma\partial_h(C_{na}F(s,u)) &= \delta\partial_h(\phi^p s^q \partial_h C_{na}) + \varepsilon\partial_h(C_{na}A(s,u)\partial_h J(s,u)), \\ \partial_t(c) + \gamma\partial_h(C_{cl}F(s,u)) &= \delta\partial_h(\phi^p s^q \partial_h C_{cl}) + \varepsilon\partial_h(C_{cl}A(s,u)\partial_h J(s,u)), \\ \partial_t(x) + \gamma\partial_h(C_{ca}F(s,u)) &= \delta\partial_h(\phi^p s^q \partial_h C_{ca}) + \varepsilon\partial_h(C_{ca}A(s,u)\partial_h J(s,u)), \\ \partial_t(y) + \gamma\partial_h(C_{so}F(s,u)) &= \delta\partial_h(\phi^p s^q \partial_h C_{so}) + \varepsilon\partial_h(C_{so}A(s,u)\partial_h J(s,u)), \\ \partial_t(z) + \gamma\partial_h(C_{mg}F(s,u)) &= \delta\partial_h(\phi^p s^q \partial_h C_{mg}) + \varepsilon\partial_h(C_{mg}A(s,u)\partial_h J(s,u)), \\ \partial_t u &= 0, \\ \partial_t v &= 0, \\ \partial_t w &= 0.\end{aligned} \tag{99}$$

That is, the model we solve for $t \in (0, \Delta t]$ is in the form

$$\begin{aligned}\partial_t\mathbf{C} + \partial_h\mathbf{F}(\mathbf{C},u) &= \partial_h(\mathbf{D}(s)\partial_h\mathbf{C}) + \partial_h(\mathbf{A}(\mathbf{C},u)\partial_h J(s,u)), \\ \mathbf{C}(\cdot,0) &= \mathbf{C}^{n+1/2}(\cdot), \quad \mathbf{U}(\cdot,t) = \mathbf{U}^{n+1/2}(\cdot)\end{aligned} \tag{100}$$

for suitable choices of $\mathbf{F}$, $\mathbf{D}$, and $\mathbf{A}$. From this we find $(\mathbf{C}^{n+1}, \mathbf{U}^{n+1}) = D_{\Delta t}(\mathbf{C}^{n+1/2}, \mathbf{U}^{n+1/2})$. For the numerical method that is used to solve this system we refer to the previous works [16, 44].

Remark 3. The following Strang splitting [17, 41] is used:

$$(\mathbf{C}^{n+1}, \mathbf{U}^{n+1}) = [D_{\Delta t/2} S_{\Delta t} D_{\Delta t/2}](\mathbf{C}^n, \mathbf{U}^n). \tag{101}$$

We do no attempt to optimize the numerical method we apply. Main focus, at this stage, is on basic properties of the model itself in terms of its capability to capture important coupled two-phase flow and water-rock interactions and corresponding behavior for the oil recovery curves, as observed through laboratory experiments.

Ions	FW [mol/l]	SW-0xSo [mol/l]	SW [mol/l]	SW-4xSo [mol/l]
Na^+	0.6849	0.474	0.450	0.378
Cl^-	1.1975	0.597	0.525	0.309
Ca^{2+}	0.2318	0.013	0.013	0.013
Mg^{2+}	0.0246	0.045	0.045	0.045
SO_4^{2-}	0	0	0.024	0.096
Ion Strength I_0	1.495	0.652	0.652	0.652

TABLE 1. Composition of the different brines used for the case where we study the effect of increasing the concentration of SO_4^{2-} ions.

Ions	FW [mol/l]	SW-0xMg [mol/l]	SW [mol/l]	SW-4xMg [mol/l]
Na^+	0.6849	0.450	0.450	0.450
Cl^-	1.1975	0.435	0.525	0.743
Ca^{2+}	0.2318	0.013	0.013	0.013
Mg^{2+}	0.0246	0	0.045	0.154
SO_4^{2-}	0	0.024	0.024	0.024
Ion Strength I_0	1.495	0.517	0.652	0.979

TABLE 2. Composition of the different brines used for the case where we study the effect of increasing the concentration of Mg^{2+} ions.

7. **Numerical investigations.** In the following we shall study the behavior predicted by the model for spontaneous imbibition with a series of different brines. We do not perform a comparison against specific experimental data. This would require that the experimental setup and the model was more consistent. Most experiments have been carried out in a setting that would require modeling in a 3D geometry. In addition, we don't have access to the relative permeability and capillary pressure curves relevant for such experiments as those reported in [46, 47]. However, much can be learnt by exploring the generic behavior of the model proposed in this work. Of particular interest, as stated in the introduction, is to gain a more accurate understanding of the oil recovery curve considered as a function of the brine composition. More precisely, the following different cases are explored.

- The effect on the oil recovery for increasing concentrations of SO_4^{2-} at a fixed temperature of $T = 130°C$ (Section 7.3).
- The effect on the oil recovery for increasing concentrations of Mg^{2+} at a fixed temperature of $T = 130°C$ (Section 7.4).
- The effect on the oil recovery when using seawater at different temperatures $T = 25°$, $T = 70°$, and $T = 130°C$ (Section 7.5).

In addition to the oil recovery curves, we employ the model to bring forth visualizations of the water-rock interplay taking place inside the core which generates changes in ion and mineral concentrations, alterations of the wetting state, and a corresponding liberation of oil.

Act coeff	γ_{ca}	γ_{so}	γ_{mg}	γ_{na}	γ_{cl}	γ_{h}	γ_{oh}	γ_{co}	γ_{hco}
SW	0.160	0.099	0.220	0.560	0.513	0.706	0.538	0.114	0.560
SW-0xMg	0.174	0.112	0.233	0.579	0.535	0.714	0.558	0.127	0.579
SW-4xMg	0.140	0.079	0.201	0.531	0.477	0.692	0.505	0.094	0.531
SW-0xSo	0.160	0.099	0.220	0.560	0.513	0.706	0.538	0.114	0.560
SW-4xSo	0.160	0.099	0.220	0.560	0.513	0.706	0.538	0.114	0.560

TABLE 3. Activity coefficients for the different brines.

7.1. **Various data needed for the simulation of laboratory core plug experiments.** Different input parameters must be specified for the model, both related to the flow and the chemical reactions. However, we emphasize that we will use a *fixed* set of parameters for all simulations unless anything else is clearly stated. The only change from one simulation to another is the brine composition.

Activity coefficients. Along the line of the previous work [16] the following values, taken from [12, 21], are used for the constants a_i^0:

$$\begin{aligned} &a_h^0 = 9, \quad a_{oh}^0 = 3.5, \quad a_{ca}^0 = 6, \quad a_{hco}^0 = 4, \\ &a_{na}^0 = 4, \quad a_{cl}^0 = 3, \quad a_{mg}^0 = 8, \quad a_{so}^0 = 4, \quad a_{co} = 4.5. \end{aligned} \tag{102}$$

Moreover, we shall use the following values for $A(T)$ and $B(T)$ taken from [12, 21]:

$$A(T = 130) = 0.6623, \qquad B(T = 130) = 0.3487. \tag{103}$$

Moreover, the following solubility products are used:

	T=25	T=70	T=90	T=130
K^c	$10^{+1.86}$	$10^{+1.21}$	$10^{+0.92}$	$10^{+0.35}$
K^g	$10^{-4.3}$	$10^{-4.87}$	$10^{-5.21}$	$10^{-5.94}$
K^m	$10^{+2.3}$	$10^{+1.24}$	$10^{+0.79}$	$10^{-0.01}$
K	$10^{-7.87}$	$10^{-8.05}$	$10^{-8.33}$	$10^{-9.01}$
C_w	$10^{-14.05}$	$10^{-12.72}$	$10^{-12.47}$	$10^{-12.26}$
C_2	$10^{-10.32}$	$10^{-10.09}$	$10^{-10.08}$	$10^{-10.15}$

K^c, K^g, K^m refer to (24)–(27), K refer to (13), C_2 refer to (14), and C_w to (15). In order to calculate C_1 in (13), we have used the given K value from the above table and the CO_2 partial pressure P_{CO_2} constant is set to $P_{CO_2} = 10^{-3.5}$, see also [28]. All these constants have been taken from the EQAlt-simulator [12, 21, 22].

Core properties. The following core properties are assumed for the model example studied below.

- Length: $L = 0.04\,\mathrm{m}$
- Porosity: $\phi = 0.4$
- Volume of core: $V_c = 75\,\mathrm{ml}$
- Volume of matrix: $V_m = 45\,\mathrm{ml}$
- Mass of rock: $M_c = 100\,\mathrm{g}$
- Permeability: $\kappa = 5\,\mathrm{mD} = 5 \cdot 0.987 \cdot 10^{-15}\,\mathrm{m}^2$.

In view of the fact that the molecular weight of $CaCO_3$ is 100g/mol, it follows that the solid part of the core corresponds to 1 mol $CaCO_3$. Consequently, the molar density is $\rho_c = 1/V_c\,\mathrm{mol/liter} \approx 13\,\mathrm{mol/liter}$.

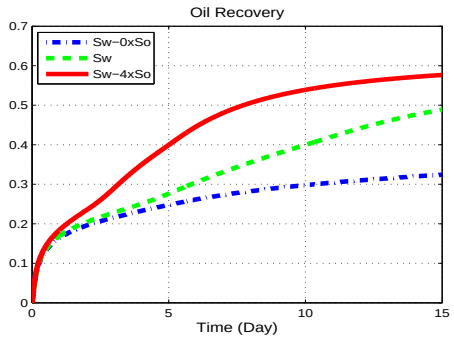

FIGURE 4. Temperature $T = 130°$C. The impact of SO_4^{2-} ions on the oil recovery.

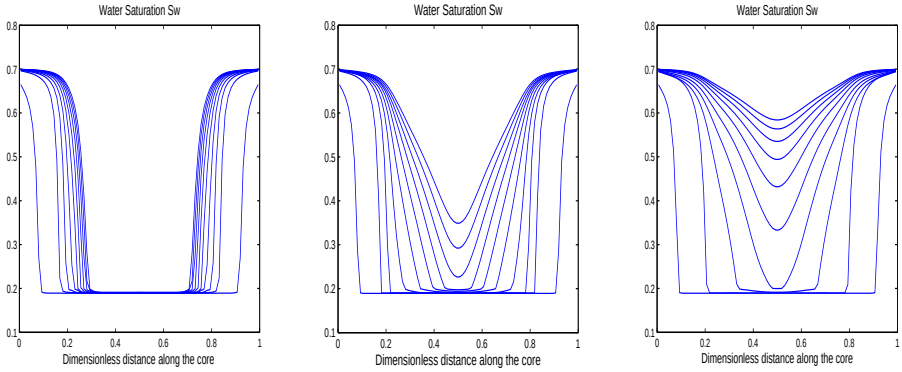

FIGURE 5. Temperature $T = 130°$C. Plots showing the water saturation s along the core at different times during a time period of 15 days. **Left**: $0xSO_4^{2-}$. **Middle**: $1xSO_4^{2-}$. **Right**: $4xSO_4^{2-}$.

Oil and brine properties.

- Oil viscosity: $\mu_o = 0.6$ cp (1 cp $= 10^{-3}$ Pa s)
- Oil density : $\rho_o = 0.73$ g/cm^3
- Water viscosity: $\mu = 0.3$ cp
- Water density: $\rho = 0.92$ g/cm^3.

Other quantities.

- Reference molecular diffusion: $D_m = \overline{D}_m = 5 \cdot 10^{-9}$ m^2/s.
- Reference capillary pressure: $\overline{P}_c = 2 \cdot 10^4$ Pa.
- Reference viscosity: $\overline{\mu} = 10^{-3}$ Pa s.

In addition, for all simulations we have used the choice $p = q = 1.9$ in the expression for molecular diffusion given by (60). Oil recovery is defined as

$$\text{Oil Recovery} := \frac{\int_0^1 [s(x,t) - s_{\text{init}}(x)]\,dx}{\int_0^1 [1 - s_{\text{init}}(x)]\,dx},$$

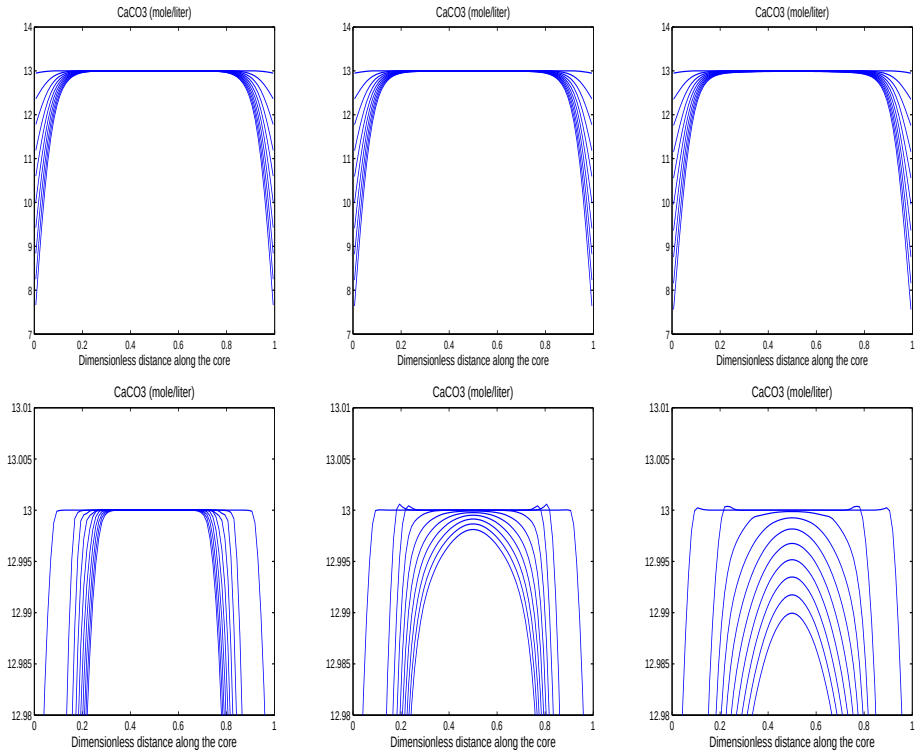

FIGURE 6. Temperature $T = 130°\text{C}$. Plots showing the dissolution/precipitation of $CaCO_3$ along the core at different times during a time period of 15 days. **Left**: $0x\text{SO}_4^{2-}$. **Middle**: $1x\text{SO}_4^{2-}$. **Right**: $4x\text{SO}_4^{2-}$. Bottom figures show zoomed in results and clearly reflect that the spreading of dissolution into the core is strongly linked to the concentration of SO_4^{2-}. Note also that one and the same brine can give dissolution at some places and precipitation at others.

where $s_{\text{init}}(x)$ is initial water saturation in the core. The reaction rate constants are set as follows:

$$k_1^c = 1.2 \cdot 10^{-5},\ k_1^g = 0.001 k_1^c,\ \text{and}\ k_1^m = 0.2 k_1^c \ \ \text{(in terms of (mol/liter))}. \quad (104)$$

These parameters are kept constant for all simulations. The values are in a similar range as those used in [16] where a brine flow-reaction model (based on the same chemical modeling as used in the present work) was compared with experimental data for flooding tests with chalk cores.

7.2. **Generally about the imbibition examples.** We simulate spontaneous imbibition for a period of time of T=15 days. Both ends of the core plug are open to the brine, and for the sake of simplicity we have neglected the impact from gravity, i.e., we set $\gamma = 0$ in (86)–(88). This is due to the fact that our main objective is to understand the relation between water-rock interaction and liberation of oil due to wettability alteration with capillarity as the driving force.

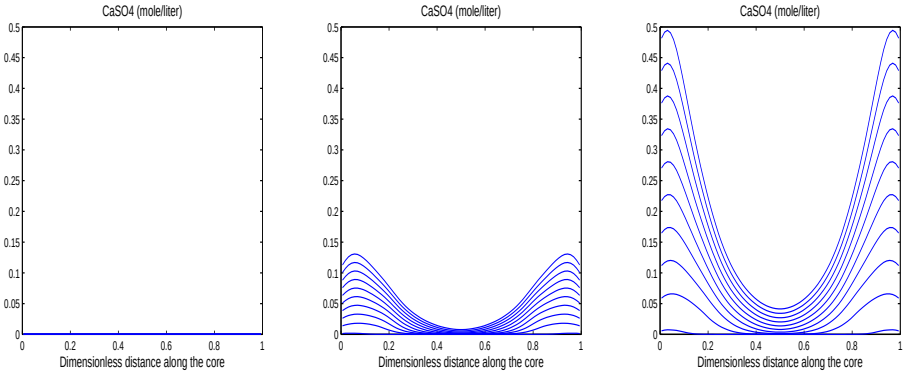

FIGURE 7. Temperature $T = 130°\text{C}$. Plots showing the precipitation of $CaSO_4$ along the core at different times during a time period of 15 days. **Left**: $0xSO_4^{2-}$. **Middle**: $1xSO_4^{2-}$. **Right**: $4xSO_4^{2-}$. The precipitation of $CaSO_4$ (which becomes stronger for a higher concentration of SO_4^{2-} in the brine) is a driving force for the dissolution of $CaCO_3$ further into the core, see Fig. 6.

The starting point for the simulation cases is that the core is (preferential) oil-wet at initial time and characterized by oil-wet relative permeability and capillary pressure curves, as described in Remark 1. The initial water saturation is set to be $s_{\text{init}}(x) = 0.191$. This corresponds to the point where oil-wet capillary pressure is zero. As a consequence, no water will imbibe into the core, hence, no oil will be produced. However, molecular diffusion will drive ions from the surrounding brine into the core. This creates concentrations fronts that move towards the center of the core bringing forth a non-equilibrium state for the water-rock system in question. This will trigger dissolution/precipitation, and the places in the core which experience dissolution of calcite will be altered towards a more water-wet surface. Consequently, capillary pressure becomes positive at these regions and water will be imbibed and oil produced to bring the system towards a new equilibrium with respect to capillary forces.

We assume that the chalk core is mainly composed of $CaCO_3$ (calcite). Hence, the following total concentrations (mol/liter) are given initially for the minerals:

$$\rho_{c,0} = 13, \qquad \rho_{g,0} = 0, \qquad \rho_{m,0} = 0.$$

The core is assumed to be filled with formation water (Ekofisk formation water) as given by Table 1. We use the ion concentrations of the imbibing brine to calculate the ionic strength I_0 given by (12). This in turn allows us to calculate the various activity coefficients from (11) by using (102) and (103). We refer to Table 3 for details.

7.3. **The role of SO_4^{2-}.** We have run three cases corresponding to the brines SW, SW-0xSo, and SW-4xSo as described in Table 1. These concentrations are similar to those used in [46] for experimental investigations. The main purpose is to study the effect on the oil recovery when the concentration of SO_4^{2-} ions is increased.

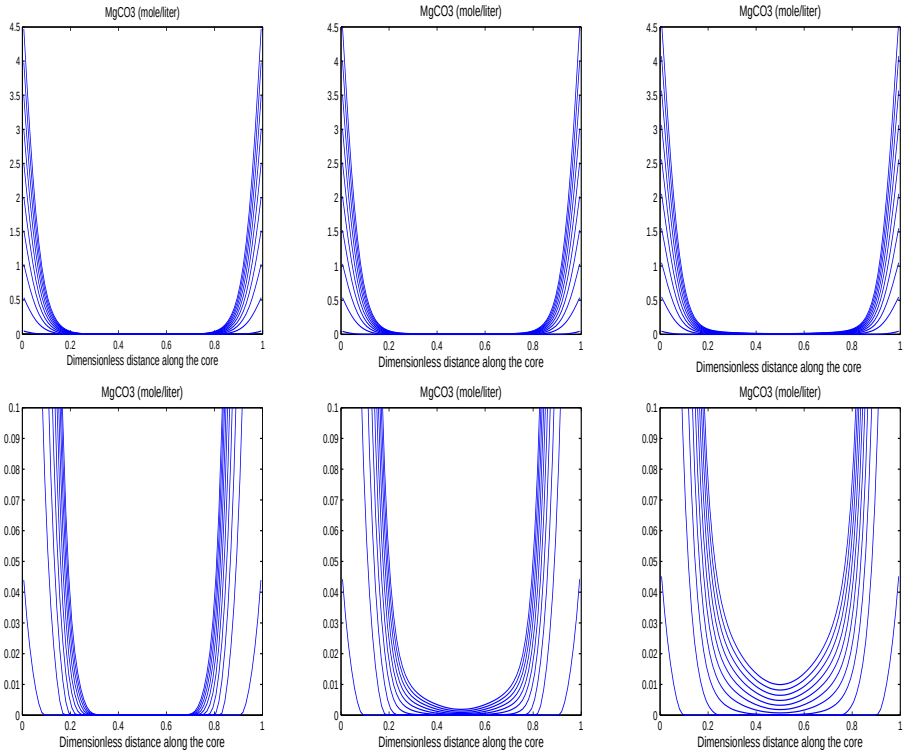

FIGURE 8. Temperature $T = 130°$C. Plots showing the precipitation of $MgCO_3$ along the core. **Left**: $0x\mathrm{SO}_4^{2-}$. **Middle**: $1x\mathrm{SO}_4^{2-}$. **Right**: $4x\mathrm{SO}_4^{2-}$. Bottom figures show zoomed in results and demonstrate that precipitation of magnesite is correlated to dissolution of calcite, compare with Fig. 6.

Oil recovery and behavior for water saturation s. The oil recovery curves corresponding to the three different brines are shown in Fig. 4 whereas the corresponding water front behavior for the three cases are shown in Fig. 5. Main observations are:

- Clearly, the concentration of SO_4^{2-} has a strong impact on the oil recovery. In particular, the brine with no sulphate gives an oil recovery level that is much lower than for the brine with 4 times seawater content of SO_4^{2-} ions. The difference between the oil recovery curves seems to remain constant after some time, at least for the two extremes corresponding to SW-0xSo and SW-4xSo, similar to the experimental curves in Fig. 1 (left figure).
- The profiles for the water saturation s for different times shown in Fig. 5 explain the oil recovery curves in Fig. 4. When no sulphate is present, the imbibing water front will gradually move slower and slower as time is running (left figure). The wettability alteration is not allowed to spread throughout the core but is limited to the end regions. However, when sulphate is present, there is a wettability alteration taking place more or less throughout the whole core with a corresponding liberation of oil (see middle and right figure).

Changes in mineral composition. Figs. 6–8 reflect the changes in the mineral concentrations for $CaCO_3$ (calcite), $CaSO_4$ (anhydrite), and $MgCO_3$ (magnesite) during the period of 15 days.

- At first sight, the upper row of figures in Fig. 6, seems to reflect that the degree of dissolution of calcite is very much the same for all three brines. The driving force behind this dissolution is the presence of Mg^{2+} ions that trigger precipitation of magnesite, see Fig. 8. However, the bottom row of figures in Fig. 6, showing the zoomed in dissolution/precipitation of calcite inside the core, reveals the intricate role played by SO_4^{2-}: It determines how far into the core the dissolution can go and thereby, by the construction of the weighting function H as described in Section 4.2 and 4.3, it also determines how far into the core the wettability alteration will go.
- Fig. 7 shows that precipitation of anhydrite $CaSO_4$ is a driving force for dissolution of calcite $CaCO_3$ in the *center* of the core. On the other hand, the strong precipitation of magnesite $MgCO_3$ close to the outlets where the core is in direct contact with the imbibing brine, see Fig. 8, is responsible for the dissolution of calcite at the ends of the core.

To sum up: The calculated solutions for the minerals clearly show how the concentration of SO_4^{2-} ions in the imbibing brine can play a role as a catalyst for the spreading of wettability alteration further into the core when it is linked to calcite dissolution.

Ion concentration profiles. Figs. 9–11 show the concentration profiles for Ca^{2+}, SO_4^{2-}, and Mg^{2+} at different times throughout the time period of 15 days. In particular, it is observed that steady state profiles are reached after some time. These steady state profiles depend on the brine composition. In other words, each brine has a set of steady state profiles, respectively, for Ca^{2+}, SO_4^{2-}, and Mg^{2+}. The corresponding set of mineral concentrations, see Fig. 6–8, reflect changes in the mineral composition. As described in Section 4, changes in the calcite mineral on the surface rock is applied as a measure for the wettability alteration that takes place, and explains why different levels of oil recovery are reached. See the figure text for more comments on the resulting ion concentration profiles.

7.4. **The role of Mg^{2+}.** We have run three cases corresponding to the brines SW-0xMg, SW, and SW-4xMg as described in Table 2. The main purpose is to study the effect on the oil recovery when the concentration of Mg^{2+} ions is increased. The results are shown in Fig. 12–19.

Oil recovery and behavior for water saturation s. The oil recovery curves corresponding to the three different brines are shown in Fig. 12 and corresponding behavior for the imbibition of water is shown in Fig. 13. Main observations are:

- The presence of Mg^{2+} ions in the imbibing brine is essential for the resulting oil recovery curve. When the brine contains no Mg^{2+} ions the water front gradually stops, practically speaking, indicating that the wettability alteration is limited to the ends of the core. This is confirmed by the results of Fig. 14 which illustrate where the dissolution of calcite takes place inside the core.
- A higher concentration of Mg^{2+} in the brine will result in a higher oil recovery, which coincides with the experimental behavior reflected by Fig. 1 (right).

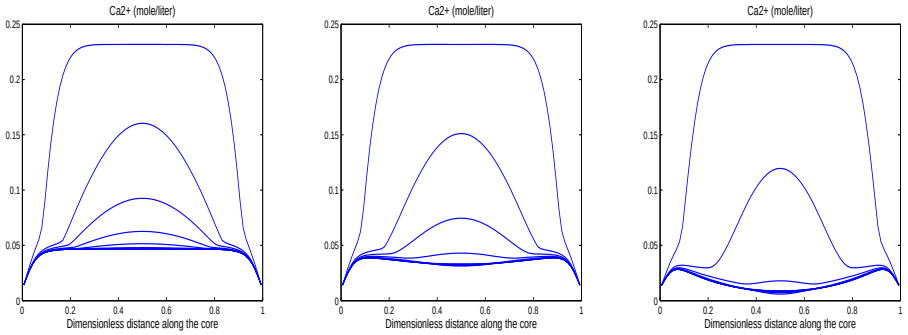

FIGURE 9. Temperature $T = 130°$C. Plots showing the concentration of Ca^{2+}. **Left**: $0x SO_4^{2-}$. **Middle**: $1x SO_4^{2-}$. **Right**: $4x SO_4^{2-}$. Steady state profiles are reached after some time. The stronger precipitation of $CaSO_4$ that follows a brine with higher concentration of SO_4^{2-} ions consumes more Ca^{2+} ions leading to the "dump" located at the center of the core. Initial concentration of Ca^{2+} is 0.23 (FW).

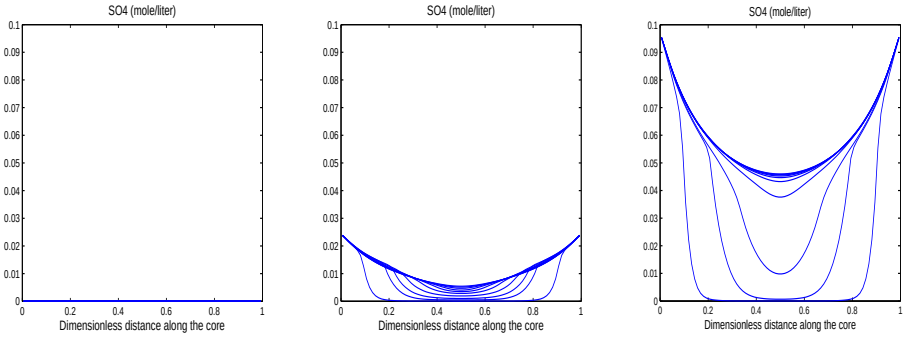

FIGURE 10. Temperature $T = 130°$C. Plots showing the concentration of SO_4^{2-} along the core at different times. **Left**: $0x SO_4^{2-}$. **Middle**: $1x SO_4^{2-}$. **Right**: $4x SO_4^{2-}$. Convergence to steady state profiles are shown reflecting that there is a considerable consumption of SO_4^{2-}, when present, due to precipitation of $CaSO_4$, compare with Fig. 7. Initial concentration of SO_4^{2-} is 0 (FW).

Changes in mineral composition.

- As shown in Fig. 14 the dissolution of calcite is largely determined by the concentration of Mg^{2+}. In particular, when Mg^{2+} ions are absent in the imbibing brine (left figure) there is a small dissolution of calcite due to precipitation of anhydrite, see Fig. 15 (left), however it is restricted to the end regions of the core. As the concentration of Mg^{2+} increases the precipitation of magnesite, see Fig. 16 (middle and right figure), will take place deeper into the core and generate a corresponding dissolution of calcite.

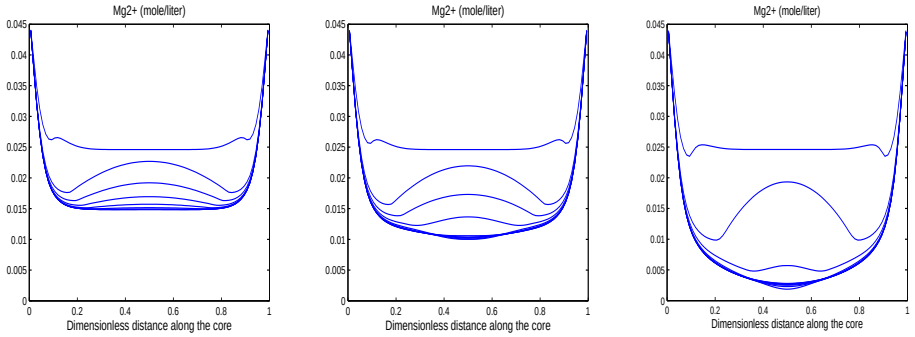

FIGURE 11. Temperature $T = 130°$C. Plots showing the concentration of Mg^{2+} along the core at different times. **Left**: $0xSO_4^{2-}$. **Middle**: $1xSO_4^{2-}$. **Right**: $4xSO_4^{2-}$. Convergence to steady state profiles are shown reflecting that more Mg^{2+} are consumed due to precipitation for higher concentration of SO_4^{2-} in the brine, compare with Fig. 8. Initial concentration of Mg^{2+} is 0.025 (FW).

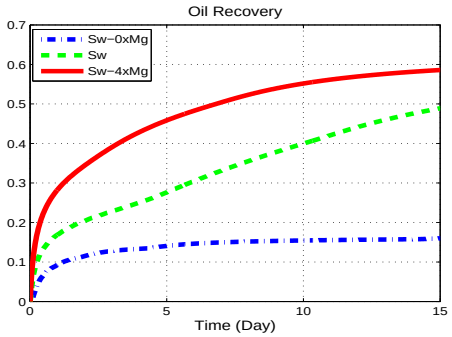

FIGURE 12. Temperature $T = 130°$C. The impact of Mg^{2+} ions on the oil recovery.

- In turn this generates a wettability alteration, not only close to the outlets, but also deeper into the core that is responsible for the increased liberation of oil.

To sum up: The calculated solutions for the minerals clearly demonstrate how the concentration of Mg^{2+} ions in the imbibing brine can act as a driving force for changing the wetting state towards water-wetness deeper into the core, and thereby increasing the oil recovery.

Ion concentration profiles. As for the previous example we observe that steady state ion concentration profiles for Ca^{2+}, SO_4^{2-}, and Mg^{2+} are obtained after some time. These steady state profiles depend directly on the brine composition. For more details, see Fig. 17–19 and corresponding figure text.

7.5. **The role of temperature on seawater as the imbibing brine.** In the final example we consider seawater as the imbibing brine. More precisely, we calculate solutions for three different temperatures, $T = 25$, $T = 70$, $T = 130°$ C. In the model

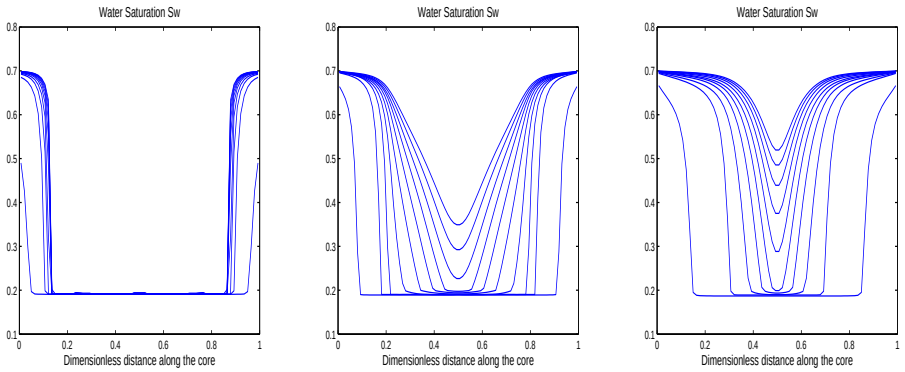

FIGURE 13. Temperature $T = 130°\text{C}$. Plots showing the water saturation s along the core at different times. **Left**: $0x\text{Mg}^{2+}$. **Middle**: $1x\text{Mg}^{2+}$. **Right**: $4x\text{Mg}^{2+}$. Note how oil is liberated in a heterogenous manner in the left figure.

we only change the solubility products according to the table given in Section 7.1. This is clearly a simplification of reality (molecular diffusion, reaction rate constants, etc. depend on temperature), however, it is of interest to see the impact on the produced oil recovery curves. These curves are shown in Fig. 20 and clearly reflect that the model will give different oil recovery levels depending on the temperature when wettability alteration is linked to water-rock interaction in terms of dissolution of calcite. In particular, in accordance with the experimental result shown in Fig. 1 (right) higher temperature gives higher oil recovery.

7.6. **A concluding remark.** The proposed model suggests that different brines give different steady-state type of solutions for the involved water-rock system. These long time solutions consist of steady state ion concentration distributions along the core together with corresponding dissolution/precipitations fronts. By letting the wettability alteration be related to these long time solutions, more precisely, the dissolution of calcite, the model naturally produce oil recovery curves as a function of brine composition that fits well with trends observed from imbibition experiments carried out in a lab setting.

REFERENCES

[1] D. Aregba-Driollet, F. Diele and R. Natalini, *A mathematical model for the sulphur dioxide aggression to calcium carbonate stones: Numerical approximation and asymptotic analysis*, SIAM J. Appl. Math., **64** (2004), 1636–1667.

[2] G. Ali, V. Furuholt, R. Natalini and I. Torcicollo, *A mathematical model of sulphite chemical aggression of limestones with high permeability. Part I. Modeling and qualitative analysis*, Transport Porous Med, **69** (2007), 109–122.

[3] G. Ali, V. Furuholt, R. Natalini and I. Torcicollo, *A mathematical model of sulphite chemical aggression of limestones with high permeability. Part II. Numerical approximation*, Transport Porous Med, **69** (2007), 175–188.

[4] T. Austad and D. C. Standnes *Wettability and Oil recovery from Carbonates: Effects of temperature and potential determining ions*, J. Pet. Sci. Eng., **39** (2003), 363–376.

[5] T. Austad, S. Strand, E. J. Hœgnesen and P. Zhang, "Seawater as IOR Fluid in Fractured Chalk," Paper SPE 93000, presented at the 2005 SPE International Symposium on Oilfield Chemistry held in Houston, Texas, USA, 2-4 February.

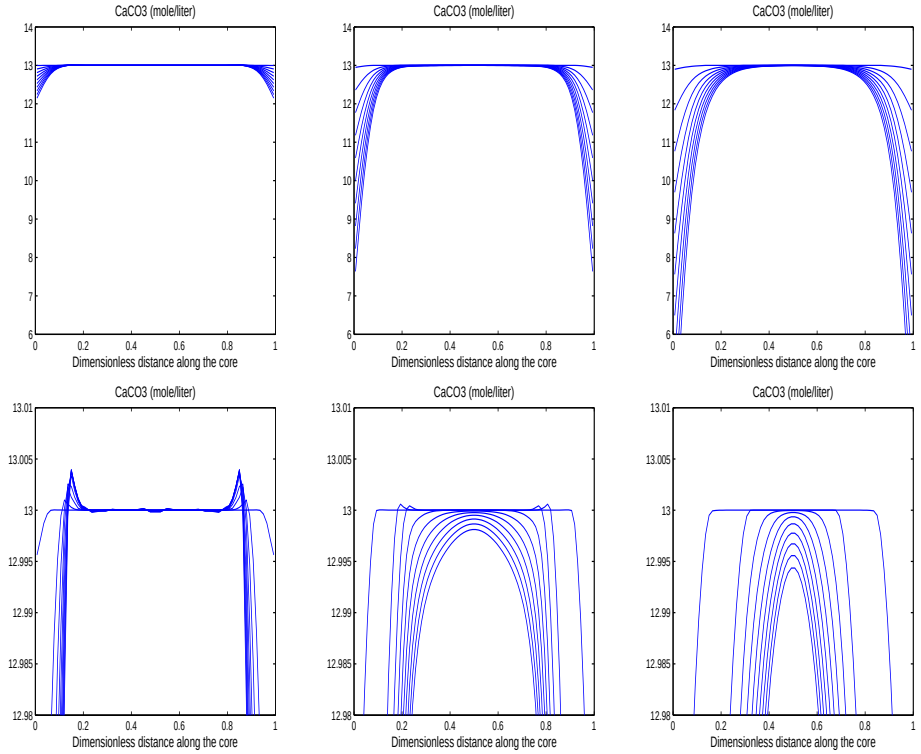

FIGURE 14. Temperature $T = 130°\text{C}$. Plots showing the dissolution/precipitation of $CaCO_3$ along the core at different times. **Left**: $0x\text{Mg}^{2+}$. **Middle**: $1x\text{Mg}^{2+}$. **Right**: $4x\text{Mg}^{2+}$. Bottom figures show zoomed in results and demonstrate how the dissolution of calcite will move into the core depending on the concentration of Mg^{2+} ions in the imbibing brine. Note the shift between dissolution and precipitation when Mg^{2+} is absent in the brine (left figure).

[6] G. I. Barenblatt, V. M. Entov and V. M. Ryzhik, "Theory of Fluid Flows Through Natural Rocks," Kluwer Academic Publisher, 1990.
[7] J. Bear, "Dynamics of Fluids in Porous Media," Elsevier, Amsterdam, 1972.
[8] P. Bedrikovetsky, "Mathematical Theory of Oil and Gas Recovery with Applications to ex-USSR Oil and Gas Fields," Petroleum Engineering & Development Studies, Vol **4**, Kluwer Academic Publishers, 1993.
[9] N. Bouillard, R. Eymard, R. Herbin and P. Montarnal, *Diffusion with dissolution and precipitation in a porous medium: Mathematical analysis and numerical approximation of a simplified model*, ESAIM: M2AN, **41** (2007), 975–1000.
[10] N. Bouillard, R. Eymard, M. Henry, R. Herbin and D. Hilhorst, *A fast precipitation and dissolution reaction for a reaction-diffusion system arising in a porous medium*, Nonlinear Analysis: Real World Applications, **10** (2009), 629–638.
[11] D. Boyd, K. Al Nayadi, et al. *Validating laboratory measured archie saturation exponents using non-resistivity based methods*, Paper prepared for presentation at the Society of Core Analysts held in Abu Dhabi, UAE, 5-9 October 2004.
[12] L. M. Cathles, "EQAlt–Equilibrium Chemical Alteration. Combined Physical and Chemical Geofluids Modeling," University of Windsor, Windsor, Ontario, 2006.

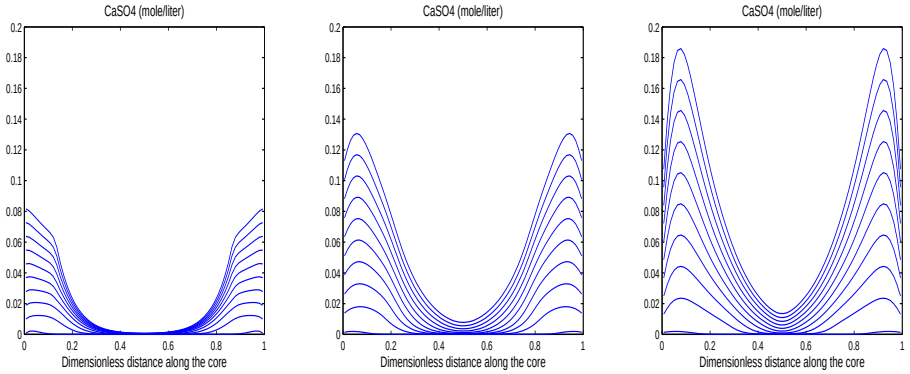

FIGURE 15. Temperature $T = 130°$C. Plots showing the precipitation of $CaSO_4$ (anhydrite) along the core at different times. **Left**: $0x\mathrm{Mg}^{2+}$. **Middle**: $1x\mathrm{Mg}^{2+}$. **Right**: $4x\mathrm{Mg}^{2+}$. The precipitation of anhydrite becomes stronger with higher concentration of Mg^{2+} ions in the imbibing brine.

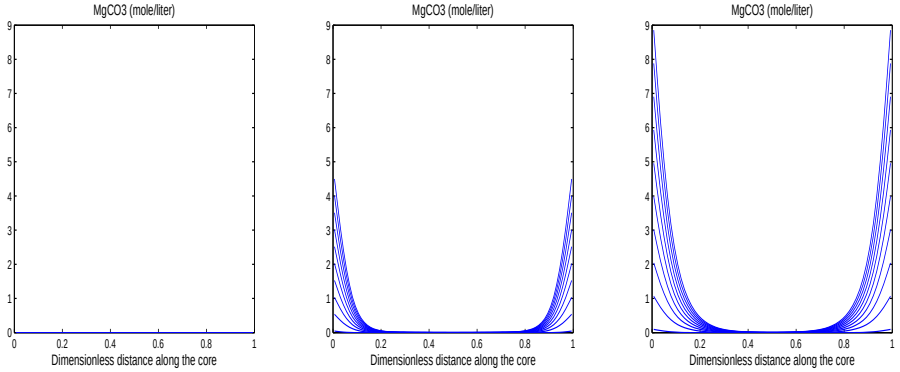

FIGURE 16. Temperature $T = 130°$C. Plots showing the precipitation of $MgCO_3$ along the core at different times. **Left**: $0x\mathrm{Mg}^{2+}$. **Middle**: $1x\mathrm{Mg}^{2+}$. **Right**: $4x\mathrm{Mg}^{2+}$. The precipitation of magnesite is strongly accelerated when the concentration of Mg^{2+} ions increases in the imbibing brine.

[13] J. Chadam, A. Peirce and P. Ortoleva, *Stability of reactive flows in porous media: Coupled porosity and viscosity changes*, SIAM J. Appl. Math., **51** (1991), 684–692.

[14] J.-S. Chen and C.-W. Liu, *Numerical simulation of the evolution of aquifer porosity and species concentrations during reactive transport*, Computers & Geosciences, **28** (2002), 485–499.

[15] Z. Chen, G. Huan and Y. Ma, "Computational Methods for Multiphase Flows in Porous Media," SIAM Computational Science & Engineering, Philadelphia, 2006.

[16] S. Evje, A. Hiorth, M. V. Madland and R. Korsnes, *A mathematical model relevant for weakening of chalk reservoirs due to chemical reactions*, Networks and Heterogeneous Media, **4** (2009), 755–788.

[17] B. Faugeras, J. Pousin and F. Fontvieille, *An efficient numerical scheme for precise time integration of a diffusion-dissolution/precipitation chemical system*, Math. Comp., **75** (2005), 209–222.

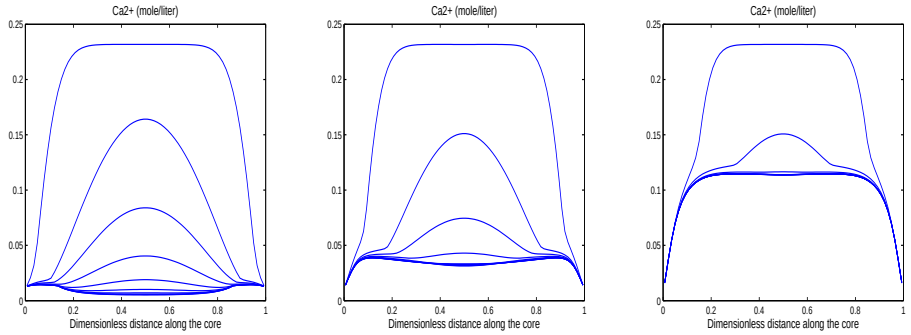

FIGURE 17. Temperature $T = 130°\text{C}$. Plots showing the concentration of Ca^{2+} along the core at different times. **Left**: $0x\text{Mg}^{2+}$. **Middle**: $1x\text{Mg}^{2+}$. **Right**: $4x\text{Mg}^{2+}$. A main characteristic is the increasing production of Ca^{2+} ions due to a stronger dissolution of calcite triggered by the stronger precipitation of magnesite when the concentration of Mg^{2+} ions increases in the imbibing brine.

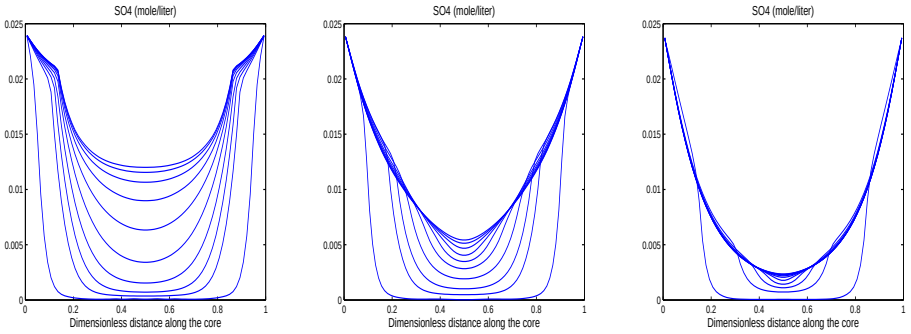

FIGURE 18. Temperature $T = 130°\text{C}$. Plots showing the concentration of SO_4^{2-} along the core at different times. **Left**: $0x\text{Mg}^{2+}$. **Middle**: $1x\text{Mg}^{2+}$. **Right**: $4x\text{Mg}^{2+}$. Increased consumption of SO_4^{2-} ions is demonstrated due to a stronger precipitation of anhydrite, compare with Fig. 15.

[18] S. S. Le Guen and A. R. Kovscek, *Nonequilibrium effects during spontaneous imbibition*, Transport Porous Med, **63** (2006), 127–146.

[19] T. Heggheim, M. V. Madland, R. Risnes and T. Austad, *A chemical induced enhanced weakening of chalk by seawater*, J. Pet. Sci. Eng., **46** (2005), 171–184.

[20] H. Helgeson, D. Kirkham, et al., *Theoretical prediction of the thermodynamic behaviour of aqueous electrolytes by high pressure and temperatures; IV*, Am. J. Sci., **281** (1981), 1249–1516.

[21] A. Hiorth, L. M. Cathles, J. Kolnes, O. Vikane, A. Lohne and M. V. Madland, "A Chemical Model for the Seawater-CO_2-Carbonate System – Aqueous and Surface Chemistry," Paper prepared for presentation at the Wettability Conference held in Abu Dhabi, UAE, 27–28 october, 2008.

[22] A. Hiorth, L. M. Cathles and M. V. Madland, *The impact of pore-water chemistry on carbonate surface charge and oil wettability*, Transport Porous Media, to appear, 2010.

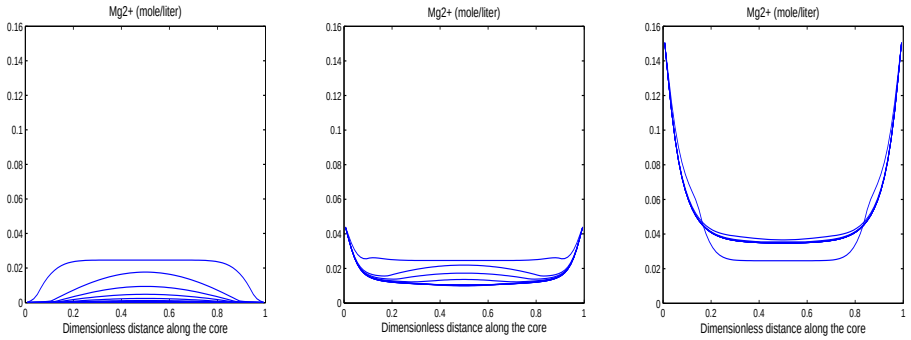

FIGURE 19. Temperature $T = 130°$C. Plots showing the concentration of Mg^{2+} along the core at different times. **Left**: $0x\mathrm{Mg}^{2+}$. **Middle**: $1x\mathrm{Mg}^{2+}$. **Right**: $4x\mathrm{Mg}^{2+}$. When Mg^{2+} ions are present in the imbibing brine (middle and right figure) there is a consumption of Mg^{2+} corresponding to the precipitation of magnesite, compare with Fig. 16.

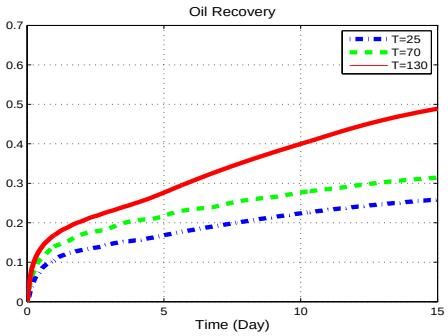

FIGURE 20. Temperature $T = 25$, $T = 70$, and $T = 130°$C. The impact of temperature on the oil recovery when seawater is used as the imbibing brine.

[23] G. R. Jerauld, C. Y. Lin, K. J. Webb and J. C. Seccombe, *Modeling low-salinity waterflooding*, SPE Reservoir Evaluation & Engineering, **11** (2008), 1000–1012.

[24] R. I. Korsnes, M. V. Madland, T. Austad, S. Haver and G. Rœsland, *The effects of temperature on the water weakening of chalk by seawater*, J. Pet. Sci. Eng., **60** (2008), 183–193.

[25] A. C. Lasaga, "Kinetic Theory in the Earth Sciences," Princeton series in geochemistry, Princeton University Press, 1998.

[26] R. J. LeVeque, "Finite Volume Methods for Hyperbolic Problems," Cambridge Texts in Applied Mathematics, Berlin, 2002.

[27] M. V. Madland, A. Finsnes, A. Alkafadgi, R. Risnes and T. Austad, *The influence of CO2 gas and carbonate water on the mechanical stability of chalk*, J. Pet. Sci. Eng., **51** (2006), 149–168.

[28] M. V. Madland et al., "Rock-Fluid Interactions in Chalk Exposed to Seawater, $MgCl_2$, and NaCl Brines with Equal Ionic Strength," 15th European Symposium on Improved Oil Recovery - Paris, France, 27–29 April 2009.

[29] J. W. Morse and R. S. Arvidson, *The dissolution kinetics of major sedimentary carbonate minerals*, Earth-Science Reviews, **58** (2002), 51–84.

[30] D. A. Nield and A. Bejan, "Convection in Porous Media," Springer Verlag, 1992.

[31] E. Oelkers and J. Schott (Editors), "Thermodynamics and Kinetics of Water-Rock Interaction," Reviews in Mineralogy & Geochemistry, **70**, 2009.
[32] A. Pawell and K.-D. Krannich, *Dissolution effects in transport in porous media*, SIAM J. Appl. Math., **56** (1996), 89–118.
[33] J. Pousin, *Infinitely fast kinetics for dissolution and diffusion in open reactive systems*, Nonlinear Analysis, **39** (2000), 261–279.
[34] J. M. Schembre and A. R. Kovscek, *Estimation of dynamic relative permeability and capillary pressure from countercurrent imbibition experiments*, Transport Porous Med, **65** (2006), 31–51.
[35] D. Silin and T. Patzek, *On Barenblatt's model of spontaneous countercurrent imbibition*, Transport Porous Med, **54** (2004), 297–322.
[36] C. I. Steefel and A. C. Lasaga, *A coupled model for transport of multiple chemical species and kinetic precipitation/dissolution reactions with application to reactive flow in single phase hydrothermal systems*, American J Sci., **294** (1994), 529–592.
[37] D. C. Standnes and T. Austad, *Wettability alteration in chalk 2. Mechanism for wettability alteration from oil-wet to water-wet using surfactants*, J. Pet. Sci. Eng., **28** (2000), 123–143.
[38] D. C. Standnes and T. Austad, *Wettability alteration in carbonate interaction between cationic surfactant and carboxylates as a key factor in wettability alteration from oil-wet to water-wet conditions*, Colloids and Surfaces A: Physicochem. Eng. Aspects, **216** (2003), 243–259.
[39] S. Strand., D. C. Standnes and T. Austad, *Spontaneous imbibition of aqueous surfactant solutions into neutral to oil-wet carbonate cores: Effects of brine salinity and composition*, Energy and Fuels, **17** (2000), 1133–1144.
[40] S. Strand, E. J. Hœgnesen and T. Austad, *Wettability alteration of carbonates-effects of potential determining ions (Ca2+ and SO42-) and temperature*, Colloids and Surfaces A: Physicochem. Eng. Aspects, **275** (2006), 1–10.
[41] G. Strang, *On the construction and comparison of difference schemes*, SIAM J. Num. Anal., **5**, (1968), 506–517.
[42] W. Stumm, "Chemistry of the Solid-Water Interface," Wiley-Interscience, 1992.
[43] I. Tripathi and K. K. Mohanty, *Instability due to wettability alteration in displacements through porous media*, Chemical Eng. Sci., **63** (2008), 5366–5374.
[44] L. Yu, S. Evje, I. Fjelde, H. Kleppe, T. Kaarstad and S. M. Skjaeveland, *Modelling of wettability alteration processes in carbonate oil reservoirs*, Networks and Heterogeneous Media, **3** (2008), 149–183.
[45] L. Yu, S. Evje, I. Fjelde, H. Kleppe, T. Kaarstad and S.M. Skjaeveland, *Spontaneous imbibition of seawater into preferentially oil-wet Chalk cores - experiments and simulations*, J. Pet. Sci. Eng., **66** (2009), 171–179.
[46] P. Zhang and T. Austad, *Wettability and oil recovery from carbonates: Effects of temperature and potential determining ions*, Colloids and Surfaces A: Physicochem. Eng. Aspects, **279** (2006), 179–187.
[47] P. Zhang, M. T. Tweheyo and T. Austad, *Wettability alteration and improved oil recovery by spontaneous imbibition of seawater into chalk: Impact of the potential determining ions Ca2+, Mg2+, and SO42-*, Colloids and Surfaces A: Physicochem. Eng. Aspects, **301** (2007), 199–208.

Received November 2009; revised March 2010.

E-mail address: steinar.evje@uis.no
E-mail address: aksel.hiorth@iris.no